PARP1 Suppression Drives ROS Resistance in Aneuploid Cancer Cells

Pan Cheng[1,2,6,7], Angela Mermerian-Baghdassarian[1,2,7], Yufeng Wang[1,2], Ze Chen[1,2], Helberth M. Quysbertf[1,2] , Pradeep Singh Cheema[4], Joseph C. Mays[1,2], Xin Zhao[1,2], Lizabeth Katsnelson[1,2], Sally Mei[1,2], Rohini Shrivastava[1,2], Mirna Bulatovic[3], Jiehui Deng[2], Markus Schober[4,5], Kwok-Kin Wong[2], and Teresa Davoli[1,2,6]

[1] Institute for Systems Genetics and Department of Biochemistry and Molecular Pharmacology, New York University School of Medicine, New York, NY, USA
[2] Division of Hematology & Medical Oncology, Laura and Isaac Perlmutter Cancer Center, New York University Langone Medical Center, New York, NY, USA
[3] Loxo Oncology at Lilly, Alexandria Center for Life Science, New York, NY, USA.
[4] Ronald O. Perelman Department of Dermatology, New York University School of Medicine, New York, NY, USA
[5] Department of Cell Biology, New York University School of Medicine, New York, NY, USA
[6] Lead Contact and Correspondence: Pan Cheng (pan.cheng.phd@gmail.com), Teresa Davoli (teresa.davoli@nyulangone.org)
[7] These authors contributed equally

Highlights

- Aneuploidy confers resistance to oxidative stress independent of p53 status, karyotype and cell lineage through inhibition of PARP1 expression and activity
- Suppressed PARP1 enhances metastatic potential, while PARP1 restoration suppresses metastatic spread, revealing a novel mechanism linking aneuploidy to cancer progression.
- PARP1 suppression compromises DNA damage repair and cell death to multiple genotoxic stressors, including reactive oxygen species, alkylating agents, and UV radiation.
- A genome-wide CRISPR screen and a CRISPRa screen identifies CEBPB as a critical transcription factor mediating PARP1 regulation and ROS resistance.
- Nuclear CEBPB increases significantly after aneuploidization in experimental systems and in primary human cancers.

Summary

Aneuploidy—defined as gains and losses of chromosomes—is frequently observed in cancer and has been implicated in promoting tumor progression and metastasis. However, the molecular mechanisms underlying this phenomenon remain poorly understood. By generating new models of aneuploidy, we found that aneuploidy confers remarkable resistance to reactive oxygen species (ROS)-mediated cell death. This resistance is a general consequence of aneuploidy, independent of the specific chromosomes gained or lost. Mechanistically, Poly(ADP-Ribose) Polymerase 1 (PARP1) is suppressed in aneuploid cells, which inhibits PARP1-mediated cell death after ROS (parthanatos). We validated aneuploidy-associated PARP1 suppression across 15 cell models and human tumors, with pronounced effects in metastatic tumors. Importantly, decreased PARP1 levels promote tumor metastasis while increased PARP1 suppresses it. Through a genome-wide CRISPR screen and functional validation, we identified the transcription factor CCAAT/enhancer-binding protein beta (CEBPB) as a critical mediator of PARP1 downregulation and ROS resistance in aneuploid cells. Furthermore, we found that lysosomal dysfunction serves as the upstream mediator of CEBPB activation in aneuploid cells. We propose that aneuploidy-driven CEBPB activation promotes PARP1 suppression, fostering ROS resistance and cancer progression.

Introduction

Aneuploidy, a hallmark of cancer[1], correlates with tumor progression, poor survival, and therapeutic resistance[2–4]. The role of aneuploidy in cancer, however, remains incompletely understood. One prevailing model proposes that aneuploidy promotes tumor-associated phenotypes by altering the dosage of oncogenes and tumor suppressors located on aneuploid chromosomes (**chromosome-specific effects**)[5–7]. The role of the aneuploid state itself (**general effects**) in promoting tumorigenesis, independent of specific chromosomal changes, is more controversial. Aneuploid cells show fitness disadvantages likely due to defects in DNA replication and proteostasis[8,9], yet resist certain chemotherapies through increased genomic instability and karyotype heterogeneity or through other mechanisms[10,11]. Whether certain general effects of aneuploidy can promote other cancer-associated phenotypes remains unclear[12–14]. A better understanding of how aneuploidy impacts tumor formation and progression could contribute to the development of effective therapies and response biomarkers.

ROS are a double-edged sword in cancer. Low-level ROS contributes to tumorigenesis and cancer development while excessive ROS during tumor progression or anti-cancer therapy can trigger cell death[15,16]. It has been recently shown that oxidative stress in circulating cancer cells

inhibits metastasis[17–19]. Therefore, cancer cells tend to enhance their ROS buffering capacity to reduce cell damage, or decrease their sensitivity to ROS-induced cell death, particularly during advanced tumor progression[17]. Interestingly, aneuploidy levels increase with tumor progression and metastasis[2,20]. However, whether a functional relationship between aneuploidy and ROS sensitivity exists and its implications for cancer progression has not been investigated.

Oxidative stress primarily induces DNA single-strand breaks (SSBs), resulting from oxidized phosphate-deoxyribose backbone fragmentation or base excision repair (BER) of oxidized bases[21]. PARP1 rapidly senses SSBs, transfers ADP-ribosyl moieties from nicotinamide-adenine-dinucleotide (NAD+) to various proteins, and facilitates the accumulation and stabilization of repair components at SSB sites[22]. Beyond DNA repair and genome integrity maintenance, PARP1 mediates a ROS-induced cell death mechanism termed parthanatos[23]. In this process, excessive oxidative DNA damage hyperactivates PARP1, depleting cells of the essential NAD+ and adenosine triphosphate (ATP)[24] and triggering nuclear translocation of mitochondrial apoptosis-inducing factor (AIF)[25], ultimately leading to cell death. Parthanatos is critical in pathophysiological processes involving cellular stress and excessive DNA damage[23,26]. For example, during cerebral ischemia, PARP1-mediated parthanatos causes neuronal cell death, which PARP1 inhibition can mitigate[27]. However, the role of parthanatos in cancer is much less well understood[28].

By studying ROS resistance in the context of cancer, we observed PARP1 suppression in aneuploid cells, which enhances resistance to ROS-induced cell death while delaying DNA damage repair. This creates a 'perfect storm' benefiting cancer cells where death resistance is coupled with compromised DNA repair. PARP1 modulation affects metastatic potential in both diploid and aneuploid cancer cells. Finally, we identified lysosomal dysfunction, a common feature of aneuploidy[29,30], activates transcription factor CEBPB, consequently suppressing PARP1 and conferring survival advantages to aneuploid cells under oxidative stress.

Results

General aneuploidy confers oxidative stress resistance in acute and chronic models of aneuploidy

To screen potential pro-tumorigenic effects of general aneuploidy (independent of specific chromosome alterations), we developed isogenic aneuploidy models. In a model of **acute aneuploidy** (**Fig. 1A**), immortalized human colon epithelial cells (hCECs) with wild-type (*TP53*WT) or knockout *TP53* (*TP53*KO) were treated with *MPS1/TTK* inhibitors (reversine or AZ3146; MPS1i) for 24-30 hours to induce chromosome missegregation[29]. Aneuploidy was confirmed by altered DNA content (**Fig. 1B**). Karyotypes inferred from single-cell RNA sequencing (see **Methods**) demonstrated that all chromosomes in MPS1i-treated *TP53*KO hCECs were gained or lost with similar frequency (25% of MPS1i-treated cells for each chromosome) (**Fig. S1A**, **Table 1A**).

107 We next compared resistance to various cellular stresses between diploid and aneuploid
108 *TP53*WT hCECs (DMSO versus MPS1i) (**Fig. 1C**, **Fig. S1B**). GFP-labeled diploid and unlabeled
109 aneuploid hCECs were treated with drugs inducing various cellular stresses, including oxidative
110 stress, proteostasis stress, energy stress, DNA damage, and metabolic stress. Inhibitors of RAC1,
111 CDKN1A, IKBKB, and MAPKs were also included (**Fig. 1C, Fig. S1B, Table 1B**). Remarkably,
112 compared to diploid ones, aneuploid cells were much more resistant to oxidative stress caused by
113 hydrogen peroxide (H_2O_2) in a concentration-dependent manner (**Fig. 1C, Fig. S1B).** Importantly,
114 H_2O_2 resistance was independent of *TP53* status (**Fig. 1D-E**).
115 To assess MPS1i off-target effects, hCECs were treated with MPS1i (or DMSO) at high
116 confluency, where cell division and aneuploidy formation are suppressed but potential off-target
117 effects remain (**Fig. S1C)**. These MPS1i-treated but non-aneuploid hCECs exhibited increased ROS-
118 induced cell death compared to controls (30-50% vs 14%) (**Fig. S1C**). This observation, along with
119 similar results from different MPS1i, suggests that ROS resistance in MPS1i-treated cells depends
120 on aneuploidy. Next, we validated this finding using other cells, including non-cancerous human
121 cells from different tissues (**Fig. S1D-E**). Furthermore, we explored the impact of the cell cycle state
122 on oxidative stress resistance. Arresting hCECs at G1 or G1/S phase (using palbociclib or
123 thymidine) increased ROS resistance in both diploid and aneuploid cells by 20-40%. However,
124 arrested aneuploid cells maintained significantly higher resistance, with ~30% greater relative
125 viability compared to diploid cells (**Fig. S1F**).
126 To examine aneuploidy effects on ROS resistance over a longer timeframe, we generated a
127 **chronic aneuploidy** model[31]. Using reversine-treated *TP53*KO hCECs, we generated 55 single-cell-
128 derived isogenic hCEC clones with varying aneuploidy levels, assessed by whole-genome
129 sequencing (**Fig. 1A, 1F**, **Table 1C**). Two representative near-diploid and four aneuploid clones (≥5
130 gains or losses of chromosomes or chromosome arms, with stable karyotypes) were compared
131 for their oxidative stress resistance (**Fig. 1F**, **Fig. S1G**). The aneuploid clones showed enhanced
132 resistance compared to near-diploid clones (**Fig. 1G, Fig. S1H-K**). Increased resistance to oxidative
133 stress was also confirmed using aneuploid clones of HCT116 (a human colon cancer cell line) and
134 RPE1[32] (**Fig. 1H**).
135 We further validated these findings by inducing aneuploidy in near-diploid mouse KP
136 (*Kras*^{G12D} and *Trp53*$^{-/-}$) lung adenocarcinoma model[33,34] using an adapted KaryoCreate strategy
137 (**Fig. 1I, S1L**). Aneuploid KP cells displayed similar proliferation but ~60% higher resistance to
138 oxidative stress compared to near-diploid controls (**Fig. 1I**), further supporting that ROS resistance
139 in aneuploid cells is not caused by cell cycle alterations. Finally, in a panel of colon cancer cell lines,
140 high-aneuploidy lines (HT29, SW403, SW948, and SK-CO-1) (**Table 1D**) were more resistant to
141 oxidative stress compared to near-diploid ones (HCT116 and DLD1) with (40-110% higher viability,
142 **Fig. 1J**, **Fig. S1M**).
143 We also confirmed aneuploidy-induced ROS resistance using alternative ROS inducers,
144 supplementing the culture medium with xanthine oxidase and xanthine to produce both O_2^-

145 (superoxide) and H_2O_2[35] (**Fig. S1N**). Collectively, our data across multiple aneuploidy models
146 provide robust evidence that aneuploidy renders cells resistant to oxidative stress, regardless of
147 *TP53* status, cell cycle, altered chromosomes, or cell lineage.
148
149
150 **Aneuploid cells resist ROS despite antioxidant levels comparable to diploid cells**
151 The aneuploidy-induced ROS resistance could result from heightened antioxidant defenses. NRF2
152 (nuclear factor erythroid 2-related factor 2) is the first-line defense against oxidative stress[17],
153 translocating to the nucleus upon activation to initiate antioxidant gene transcription[36]. We
154 examined *NRF2* activation and found that acute aneuploid hCECs showed no significant increase
155 in NRF2 nuclear translocation (**Fig. S2A**). Aneuploid hCEC clones even displayed slightly reduced
156 NRF2 nuclear translocation versus near-diploid clones. Consistently, *NRF2* knockout did not
157 abolish the survival advantage of aneuploid hCECs relative to diploid controls under oxidative stress
158 (**Fig. S2B**). Furthermore, knockdown of key antioxidant genes, *GPX1* and *CAT*, which are crucial for
159 direct cellular H_2O_2 elimination, did not abolish ROS resistance in aneuploid cells (**Fig. S2C**).
160 Collectively, these findings suggest that the increased oxidative stress resistance in aneuploid cells
161 is not mediated by enhancement of cellular antioxidant defenses via *NRF2*, *GPX1,* or *CAT*.
162 We then compared ROS-induced cellular damage between diploid and aneuploid hCECs
163 (**Fig. 2A**, **Fig. S2D-E**). Alkaline comet assay revealed that H_2O_2 exposure induced a level of DNA
164 damage (double and single-strand breaks) that is comparable or slightly higher in aneuploid versus
165 diploid hCECs **(Fig. 2A, Fig. S2D**). This result was corroborated by the similar levels of the DNA
166 damage marker phosphorylated histone H2AX (Ser139; γH2AX) between diploid and aneuploid
167 cells after H_2O_2 (see **Fig. 3M**, **Fig. S3H-K**). Furthermore, H_2O_2 exposure resulted in similar lipid
168 peroxidation levels in diploid and aneuploid hCECs (**Fig. S2E**). These findings indicate that the
169 resistance of aneuploid cells to oxidative stress is not due to enhanced antioxidant defenses, as no
170 reduction in oxidative DNA or lipid damage was observed in aneuploid compared to diploid cells
171 following H_2O_2 exposure.
172
173
174 **PARP1, a key mediator of ROS-induced cell death, is suppressed in aneuploid cells**
175
176 Since no reduction in oxidative DNA or lipid damage was observed in aneuploid cells, we
177 investigated whether aneuploid cells better resist ROS-induced cell death despite comparable
178 levels of cellular damage. To determine the specific cell death pathway activated by oxidative
179 stress, we pretreated hCECs with inhibitors of apoptosis, necrosis, ferroptosis, and PARP1-
180 mediated parthanatos (olaparib). Strikingly, only olaparib significantly rescued H_2O_2-induced cell
181 death (**Fig. 2B-C, Fig. S2F**). This indicates that elevated oxidative stress triggers parthanatos in our
182 cell model.

PARP1, the molecular target of olaparib, is crucial for parthanatos: it senses DNA damage caused by ROS or other stimuli, and in the presence of high levels of damage, it initiates parthanatos by exhausting NAD+ and ATP or by triggering AIF nuclear translocation[24,25]. Importantly, we observed a consistent decrease in PARP1 RNA (~40-50%) and protein (~50-60%) levels in aneuploid cells compared to diploid controls across multiple cell line models (**Fig. 2D-E**, **Table 2A-B),** independent of their transformation state, *TP53* status, or cell lineage. PARP1 downregulation was also observed in previous reports on reversine-treated RPE1 cells[29], glioma cells[37], and mouse embryos[38], while none of these studies focused on PARP1 or parthanatos. Furthermore, we probed for PARP1 activity and observed reduced poly(ADP-ribose) (pADPr) synthesis in MPS1i-treated aneuploid cells after H_2O_2 exposure (**Fig. S2G**). Importantly, the decline in PARP1 protein cannot be attributed to caspase-mediated cleavage[39], as it persisted with a pan-caspase inhibitor (**Fig. S2H**). It is important to highlight that *PARP1* is haploinsufficient[40], thus a partial change in gene dosage can profoundly impact cell state and function.

The negative correlation between aneuploidy degree and PARP1 expression at RNA and protein levels was also validated in the isogenic aneuploid and diploid hCEC clones (RNA: Spearman R = -0.58, p = 0.01; protein: Spearman R = -0.49, p = 0.05; **Fig. 2F-H**, **Table 2C-D**). HCT116 clones and RPE1 clones (**Fig. 2I**, **Fig. S2I-J**), each carrying different aneuploidies, exhibited lower PARP1, suggesting that PARP1 downregulation is independent of specific altered chromosomes. Finally, aneuploidy-associated PARP1 downregulation was also validated using KP lung cancer cells (**Fig. S2K**) and human colon cancer cell lines (see **Fig. 4A**). Taken together, these data suggest that PARP1 downregulation is a common feature of aneuploid cells, regardless of *TP53* status, altered chromosomes, cell lineage, or transformation state.

PARP1 suppression reduces aneuploid cell sensitivity to PARP1-mediated cell death induced by ROS, alkylating agents, or UV radiation

While *PARP1* is considered a pro-survival gene that senses DNA damage and promotes DNA repair[22], its hyperactivation can trigger parthanatos, the most common form of regulated necrosis induced by DNA damage[26,41]. Given our findings of *PARP1* suppression in aneuploid cells (**Fig. 2**), we hypothesized that this reduction contributes to their resistance to ROS-induced (or more generally, PARP1-mediated) cell death. To test this hypothesis, we modulated *PARP1* expression through knockdown/knockout or overexpression and assessed corresponding changes in cell sensitivity to H_2O_2, an activator of PARP1-mediated cell death.

shRNA- or CRISPR-mediated *PARP1* inhibition conferred H_2O_2 resistance to near-diploid hCEC clones, compared to control cells (**Fig. 3A-B**, **Fig. S3E-F**). Conversely, PARP1 overexpression decreased H_2O_2 resistance in both acutely and chronically aneuploid hCECs, reducing relative viability compared to empty vector controls (**Fig. 3C-F, Fig. S3A**). Notably, the resistance induced by the shRNA targeting *PARP1* 3'-UTR was reversed by overexpressing shRNA-resistant *PARP1*

222 cDNA (**Fig. 3G**). Consistent with observations in hCECs, *PARP1* overexpression in the high-
223 aneuploidy colon cancer cell line (HT29) reduced H_2O_2 resistance (see **Fig. 4D-E**, **Fig. S4A**), while
224 *PARP1* knockdown in the near-diploid colon cancer cell lines (HCT116 and DLD1) enhanced
225 resistance (see **Fig. 4F-G**, **Fig. S4B**). Notably, using doxycycline-inducible PARP1 expression, we
226 found that a 20% increase in PARP1 expression sufficiently reduced H_2O_2 resistance, decreasing
227 relative viability by ~20% **(Fig. 3H)**.
228 To examine additional factors that may work with PARP1 to contribute to aneuploidy-
229 associated oxidative stress resistance, we next investigated PARP1-associated proteins that have
230 been shown to promote its function. One of the most prominent is Timeless Circadian Regulator
231 (*TIMELESS*), which physically interacts with PARP1 and promotes its recruitment to DNA damage
232 foci and subsequent activation[42]. *TIMELESS* expression was consistently decreased at RNA levels
233 in acutely aneuploid cells compared to diploid controls (**Fig. S3B**) and inversely correlated with
234 aneuploidy degree at RNA and protein levels in the chronic aneuploidy model (**Fig. S3C**). We found
235 that in the highly-resistant aneuploid clone A29, co-overexpression of *PARP1* and *TIMELESS*
236 reduced H_2O_2 resistance more than overexpression of either gene alone (**Fig. 3I**, **Fig. S3D**),
237 suggesting TIMELESS downregulation may enhance ROS resistance induced by *PARP1*
238 suppression in aneuploid cells. Given the strong effect of TIMELESS overexpression on ROS
239 sensitivity, we investigated the necessity of *PARP1* downregulation in *TIMELESS*-mediated ROS
240 sensitivity. We knocked out *PARP1* in A29 cells overexpressing *TIMELESS*. Strikingly, *PARP1*
241 knockout completely abolished the sensitizing effect of *TIMELESS* overexpression on H_2O_2-induced
242 cell death (**Fig. S3L**), demonstrating that *PARP1* is the primary effector of oxidative stress
243 sensitivity and that *TIMELESS* acts through *PARP1* to modulate this response. While *PARP1*
244 catalyzes 85-95% of total cellular pADPr in response to DNA damage, *PARP2* has a similar function
245 and is also targeted by olaparib[43]. However, *PARP2* knockout did not protect hCECs from H_2O_2 (P
246 = 0.22; **Fig. S3E**), arguing against its involvement in aneuploidy resistance to parthanatos.
247 Macrophage migration inhibitory factor (*MIF*), a late-stage parthanatos nuclease, cleaves genomic
248 DNA[44]. *MIF* knockout partially protected hCECs from H_2O_2, but less effectively than *PARP1*
249 knockout (relative viability increased by 20-38% for *PARP1* knockout vs 7-14% for *MIF* knockout,
250 **Fig. S3F**).
251 Furthermore, we investigated whether mitigating NAD+ depletion, a typical consequence of
252 PARP1 hyperactivation[23,45], inhibits cell death after H_2O_2 treatment. Supplementation with
253 nicotinamide mononucleotide (NMN, a NAD+ precursor) increased the viability of H_2O_2-treated
254 hCEC clones (**Fig. 3J**). Finally, we applied agents other than H_2O_2-induced ROS to induce DNA
255 damage and PARP1 activation: N-methyl-N'-nitro-N-nitrosoguanidine (MNNG), a common
256 alkylating agent, and UV radiation, both known to trigger PARP1-mediated cell death[41]. Remarkably,
257 aneuploid hCEC clones were more resistant to these stimuli than near-diploid clones in a PARP1-
258 dependent manner (**Fig. 3K-L**). Collectively, these results suggest that PARP1 downregulation

confers resistance to PARP1-mediated cell death in aneuploid cells, whether induced by ROS, alkylating agents, or UV radiation.

PARP1-mediated DNA damage repair is impaired in aneuploid cells

Given the crucial role of *PARP1* in this process[22] and its downregulation in aneuploid cells, we investigated the impact of *PARP1* suppression on DNA damage repair in aneuploid cells. We transiently exposed isogenic near-diploid and aneuploid hCEC clones to genotoxic insults and collected cells before (control) and after stimulation (with no observed cell death prior to collection). DNA damage was assessed by measuring γH2AX[46] (**Fig. S3G**). Seven genotoxic agents inducing DNA damage through distinct mechanisms were tested: H_2O_2 (oxidative damage), MNNG (base alkylation), camptothecin (topoisomerase I inhibition), etoposide (topoisomerase II inhibition), pyridostatin (C-quadruplex stabilization), doxorubicin (DNA intercalation), and bleomycin (DNA synthesis inhibition). We found that repair of H_2O_2- and MNNG-induced DNA damage was significantly slower in aneuploid clones compared to diploid cells (see **Methods**), whereas repair of DNA damage induced by other genotoxic agents was not (**Fig. S3H-I**). After six hours of recovery from H_2O_2 treatment, median γH2AX intensity decreased by ~40% in near-diploid clones but by only 15% (A29) or increased by 20% (A20) in aneuploid clones (**Fig. S3H-I**). Similarly, MNNG-induced DNA damage repair was less efficient in aneuploid clones, with median γH2AX intensity increasing by 54-103% compared to -16% to 19% in near-diploid clones after six hours of recovery (**Fig. S3H-I**). This likely reflects the strong reliance on PARP1 for repairing H_2O_2- and MNNG-induced DNA damage, whereas other agents engage multiple, less PARP1-dependent repair pathways[46] (see **Discussion**). The suppressive effect of PARP1 downregulation on oxidative DNA damage repair was further validated by analyzing PARP1-overexpressing cells. PARP1 overexpression promoted oxidative DNA damage repair in both acute and chronic aneuploidy models (**Fig. 3M, Fig. S3J**, **Table 3**). Importantly, we excluded the possibility that γH2AX dynamics resulted from altered H2AX protein levels, as γH2AX changes were independent of total H2AX level fluctuations (**Fig. S3K**). Additionally, the γH2AX decrease in the near-diploid clones 6 hours after H_2O_2 exposure is likely unrelated to programmed cell death, as previous studies showed PARP1-mediated cell death does not cause collateral γH2AX decrease[47]. Taken together, our data indicate that aneuploid cells, besides surviving H_2O_2 or MNNG-induced cell death, may be more prone to accumulating DNA damage due to suppressed PARP1-mediated DNA repair. The combination of death resistance and DNA damage accumulation may collectively promote tumorigenesis and cancer evolution (see **Discussion**).

PARP1 downregulation promotes tumor progression of aneuploid cancer cells

298 Given the decreased PARP1 expression across different aneuploidy models (**Fig. 2**), we asked
299 whether the same was true in human cancer cell lines and in primary tumors with varying
300 aneuploidy levels. Western blot (WB) analysis of four high-aneuploidy (HT29, SW948, SK-CO-1,
301 SW403) and two near-diploid (HCT116, DLD1) colon cancer cell lines revealed lower PARP1
302 expression in high-aneuploidy lines (all cell lines have two copies of *PARP1* gene, **Fig. 4A**, **Table**
303 **1D**). Analysis of pan-cancer cell lines in the CCLE dataset, evenly grouped into three aneuploidy
304 levels, revealed significant aneuploidy-dependent decreases in PARP1 expression at both SCNA-
305 normalized RNA and protein levels (RNA mean log2FC = -0.3, protein mean log2FC = -0.25, high vs
306 low aneuploidy, $p<0.0001$, $p=0.0013$; **Fig. 4B**). This association extended to colorectal cancer cell
307 lines from the CCLE dataset (**Fig. 4C**).
308 Furthermore, consistent with our findings in hCECs that PARP1 expression inversely
309 correlates with cell resistance to ROS-induced death (**Fig. 3**), *PARP1* overexpression attenuated
310 ROS resistance in high-aneuploidy colon cancer cells (**Fig. 4D-E**, **Fig. S4A**), while *PARP1*
311 knockdown enhanced ROS resistance in near-diploid colon cancer cells (**Fig. 4F-G**, **Fig. S4B**). These
312 results further support our model, indicating that PARP1 expression levels critically determine
313 cancer cell sensitivity to ROS-induced cell death (**Fig. 3**).
314 Since metastasis requires cancer cells to withstand high oxidative stress during migration
315 and colonization[17–19,48], we investigated whether PARP1 levels influence dissemination potential of
316 diploid and aneuploid cancer cells. We found *PARP1* suppression enhanced dissemination
317 potential of near-diploid human colon cancer cells in immunodeficient mice (**Fig. 4H-I**). DLD1 and
318 HCT116 cells transduced with *PARP1* shRNA exhibited significantly increased bioluminescence
319 signals four or six weeks post-injection compared to controls with non-targeting shRNA,
320 respectively (n=5 mice per group; $p = 0.007$ for DLD1 at week 4, $p = 0.03$ for HCT116 at week 6; **Fig.**
321 **4H-I**). Importantly, *PARP1* knockdown did not affect cell proliferation *in vitro* (**Fig. S4C**).
322 Furthermore, we assessed the impact of PARP1 levels on murine aneuploid cancer cells in immune-
323 intact mice. We intravenously injected aneuploid mouse KP lung cancer cells (**Fig. 1I**, **Fig. S1J**) into
324 B6 Albino mice. Consistently, mouse PARP1 overexpression decreased their tumor dissemination
325 without affecting *in vitro* proliferation, with 40% of mice developing tumors in the PARP1 OE group
326 compared to 80% in empty vector controls (**Fig. 4J**, **Fig. S4D**). These data indicate that PARP1
327 downregulation may promote metastasis of aneuploid cancer cells in both immune-deficient and
328 immune-intact mice.
329 We next examined PARP1 levels in human primary tumors to determine whether it changes
330 with tumor stage and patient survival. In line with our *in vivo* findings, among TCGA colorectal
331 adenocarcinoma (COREAD) patients lacking PARP1 SCNA[49], PARP1 expression was lower in high-
332 versus low-aneuploidy tumors (**Fig. 4K**, **Table 4**), and lower PARP1 expression was associated with
333 shorter survival (**Fig. 4L**, **Table 4**). This aligns with previous studies showing that late-stage
334 COREAD tumors, typically characterized by higher aneuploidy degrees[50], exhibit lower PARP1
335 expression and activity compared to early-stage tumors[51]. Furthermore, we compared PARP1

levels in primary and metastatic COREAD samples and found decreased PARP1 expression in metastases compared to primary tumors in both paired ($p < 0.01$; **Fig. 4M**) and unpaired sample cohorts[52] (**Fig. 4N**, **Fig. S4E**). Altogether, these findings support a role for *PARP1* downregulation in promoting metastasis.

CRISPR screen identifies lysosomal stress is a potential mediator of PARP1 downregulation in aneuploid cells

Next, we investigated the mechanisms of *PARP1* regulation, specifically its downregulation in aneuploid cells. We conducted fluorescence-activated cell sorting (FACS)-based genome-wide CRISPR screens to identify genes modulating PARP1 expression, using endogenous PARP1 levels as the readout (**Fig. 5A-B** and **Fig. S5A**).

SgRNAs were sequenced from PARP1-low, PARP1-high, and unsorted cells. We anticipated sgRNAs targeting putative ***PARP1*** **activators** to be enriched in PARP1-low cells compared to unsorted cells, while sgRNAs targeting putative ***PARP1*** **suppressors** would be enriched in PARP1-high cells. Using MAGeCK to calculate enrichment scores for each gene, we revealed a negative correlation between gene enrichment in PARP1-low and PARP1-high populations ($p < 2e-16$, rho = -0.22, **Fig. 5C**, **Table 5A**), indicating exclusive enrichment of genes in populations with different PARP1 levels. Importantly, sgRNAs targeting *PARP1* were enriched in the PARP1-low population and depleted from the PARP1-high population (beta = 0.48 and -1.55, p-value = 0.003 and 0 for PARP1-low and PARP1-high populations, respectively; **Fig. 5C-D**), confirming the screen's success.

The screen identified 269 *PARP1* activators and 155 suppressors (FDR < 0.1, beta > 0.5, **Table 5B**). QIAGEN Ingenuity Pathway Analysis (IPA) revealed that *PARP1* activators were enriched in pathways related to phagosome maturation (p-value = 1.7e-17), tRNA charging (p-value = 3.7e-14) among others. *PARP1* suppressors were predominantly associated with RNA polymerase I complex assembly (p-value = 1.2e-6) (**Fig. 5E**, **Fig. S5B**, **Table 5C-D**).

To identify genes and pathways that may mediate PARP1 downregulation in aneuploid cells, we examined how the expression of these *PARP1* activators and suppressors changes in aneuploid compared to diploid cells (**Fig. S5C**). Aneuploidy-associated *PARP1* regulators were identified by finding *PARP1* activators that are downregulated in aneuploid cells and *PARP1* suppressors that are upregulated in aneuploid cells (**Fig. S5D, Table 5E**). Phagosome maturation pathway (p-value = 6.4e-03), consisting of many lysosome genes, was enriched in these aneuploidy-associated PARP1 regulators (**Fig. S5E**, **Table 5F**), suggesting that lysosomal dysregulation in aneuploid cells may cause PARP1 downregulation.

Lysosomal stress is characteristic of aneuploidy[29], with aneuploid cells showing transcriptional profiles similar to cells treated with the lysosomal V-ATPase inhibitor bafilomycin A1 (Baf A1)[30]. Our screen showed that knockout of lysosomal genes resulted in PARP1 downregulation (phagosome maturation pathway in **Fig. 5E** and **Fig. S5E**, individual lysosomal *V-*

375 *ATPase* genes in **Fig. S5F**). Thus, we hypothesized that aneuploidy-associated lysosomal stress
376 induces PARP1 downregulation and tested this hypothesis. First, principal component analysis
377 (PCA) of RNAseq data from 8 near-diploid and 11 aneuploid hCEC clones revealed that lysosomal,
378 but not proteasomal, genes differentiated near-diploid from aneuploid cells (p-value < 0.0001 and
379 = 0.173, respectively, **Fig. 5F**), indicating a distinct lysosomal gene expression profile in aneuploid
380 cells. Second, expression changes of these lysosomal genes and the whole transcriptome in
381 aneuploid cells correlated with those in cells treated with the lysosome inhibitor Baf A1 (Spearman
382 p-value < 0.05, **Fig. 5G-H, Fig. S5G**), suggesting that aneuploid cells experience Baf A1-like
383 lysosomal stress. Third, analysis of four published datasets[29,53–55] revealed that lysosome inhibitor
384 Baf A1 treatment reduced PARP1 expression in various cell lines (Log2FC: -0.350 to -1.112, **Fig. 5I**).
385 Reduction in PARP1 after Baf A1 treatment was further validated by WB analysis in our hCECs (**Fig.**
386 **S5H**). Conversely, proteasome inhibition[29,56–58] did not affect PARP1 expression (p-value > 0.05, **Fig.**
387 **S5I**), highlighting the specificity of lysosome inhibition for PARP1 downregulation. Finally, Baf A1
388 treatment protected hCECs (both *TP53*WT and *TP53*KO) from H_2O_2-induced cell death (91-107%
389 increase in relative viability, **Fig. 5J**). This lysosome dysfunction-induced resistance to oxidative
390 stress was eliminated by PARP1 overexpression (p-value < 0.0001, **Fig. 5K**). These results suggest
391 that lysosomal stress promotes PARP1 downregulation and corresponding oxidative stress
392 resistance in aneuploid cells.
393
394
395 **CEBPB is an aneuploidy-induced transcription factor that suppresses PARP1 expression**
396
397 Decreased PARP1 RNA levels in cells with aneuploidy or lysosomal dysfunction (**Fig. 2**, **Fig. 5**)
398 suggested that these conditions may alter *PARP1* transcription. We therefore sought to identify
399 transcription factors (TFs) that may be responsible for *PARP1* transcriptional dysregulation in these
400 settings. We integrated our PARP1 CRISPR screen (**Fig. 5C**) with TF databases[59–61] to identify TFs
401 influencing *PARP1* expression (**Fig. 6A**). Additionally, we examined expression changes of these
402 TFs in aneuploid and lysosome-dysfunction cells, searching for downregulation of TFs promoting
403 *PARP1* expression and upregulation of those suppressing *PARP1* expression (**Fig. 6A,** see
404 Methods). These analyses identified CEBPB as a potential suppressive TF of *PARP1*, with
405 consistently elevated expression in various aneuploid and lysosome-dysfunction cell models
406 (p<0.05, **Fig. 6B-F**). CEBPB ChIP-Seq[62] confirmed its binding near the *PARP1* transcription start site
407 upon activation by dexamethasone (*CEBPB* activator) (reproducible peaks identified by the
408 Irreproducibility Discovery Rate algorithm, **Fig. 6B**). IF analysis of hCECs showed a significant
409 increase in nuclear CEBPB signal in aneuploid cells compared to near-diploid cells in both the
410 chronic and acute aneuploidy models (**Fig. 6D**). CEBPB upregulation was also confirmed in our
411 transcriptomic and proteomic datasets in both acute (**Fig. 6C**) and chronic models (**Fig. 6E**).
412 Lysosome dysfunction induced by Baf A1 also increased CEBPB levels across multiple lines (**Fig.**
413 **6F**) and enhanced nuclear localization in hCECs with *TP53*WT or *TP53*KO (**Fig. S6A**). *CEBPB*

414 activation was also supported by transcription factor enrichment analysis using ChEA3 (ENCODE
415 dataset)[63], showing significant overlap between CEBPB target genes and highly upregulated genes
416 (log2FC > 1 & FDR < 0.01) in reversine-treated hCECs (ranked 3rd, FDR = 6.38E-5) and Baf A1-treated
417 RPE1 cells (ranked 5th, FDR = 2.98E-4) (**Table 6**). These convergent lines of evidence suggested
418 CEBPB activation in aneuploid and lysosome-dysfunction cells.
419 Given the established role of lysosomal stress in aneuploid cells[29], we sought to further
420 interrogate the relationship between lysosomal dysfunction and *CEBPB* activation. TFEB and TFE3
421 are key transcriptional regulators of lysosomal biogenesis[64]. To test whether further disrupting
422 autophagy by inhibiting TFEB and TFE3 would exacerbate CEBPB activation, we knocked down
423 *TFEB* or *TFE3* in diploid and aneuploid hCEC clones. Knockdown of either *TFEB* or *TFE3*
424 significantly increased nuclear CEBPB levels specifically in aneuploid cells (A20, A21, A29) but had
425 no significant effect in near-diploid cells (D23, D29) (**Fig. S6B**). This aneuploidy-specific response
426 suggests that further compromising autophagy in already-saturated aneuploid cells exacerbates
427 CEBPB activation, whereas diploid cells with intact lysosomal function are more resilient to TFEB
428 or TFE3 disruption. Consistent with the role of CEBPB in mediating oxidative stress resistance,
429 *TFEB* or *TFE3* knockdown significantly increased H_2O_2 resistance specifically in aneuploid clones
430 (A20, A21, A29), with no effect observed in near-diploid cells (D23, D29) (**Fig. S6C)**. These findings
431 establish lysosomal dysfunction as an upstream trigger of CEBPB activation.
432 Our PARP1 CRISPR screen revealed enrichment of *CEBPB*-targeting sgRNAs in the PARP1-
433 high population and depletion in the PARP1-low population (**Fig. 6G**), suggesting CEBPB's
434 suppressive role in PARP1 expression. This was further corroborated by decreased PARP1 protein
435 upon CEBPB overexpression in various cells (**Fig. 6H**), and reduced PARP1 RNA in TCGA COREAD
436 tumors with *CEBPB* amplification (excluding patients with PARP1 SCNA, $p < 0.01$, **Fig. S6D**). In a
437 recent CRISPR activation (CRISPRa) Perturb-seq screen to evaluate the impact of transcription
438 factor activation[65], cells with *CEBPB* activation via CEBPB-targeting sgRNAs exhibited higher
439 CEBPB levels and lower PARP1 levels compared to control cells (**Fig. 6I**). To directly assess
440 whether CEBPB binds to the *PARP1* promoter, we performed chromatin immunoprecipitation
441 followed by quantitative PCR (ChIP-qPCR). CEBPB showed significant enrichment at the *PARP1*
442 promoter in cells treated with dexamethasone (*CEBPB* activator) and reversine compared to DMSO
443 control (**Fig. S6E**). Collectively, these results indicate that CEBPB activation suppresses PARP1
444 expression.
445 Next, we confirmed the inverse relationship between CEBPB, PARP1, aneuploidy, and
446 lysosomal status in human primary colorectal tumors using scRNAseq[66,67]. Cells with high CEBPB
447 expression exhibited high aneuploidy scores, high lysosome scores, and low PARP1 expression,
448 and vice versa (**Fig. 6J, Fig. S6F**), revealing that aneuploid cancer cells are associated with
449 lysosomal alterations, CEBPB activation and low PARP1 expression. Consistently, we observed
450 strong inverse correlations between CEBPB and PARP1 RNA levels across pan-cancer cell lines
451 (**Fig. 6K**) and COREAD tumors (**Fig. S6G**). These associations across our models and human

452 datasets, combined with the functional validation of *CEBPB* knockout or overexpression on PARP1
453 expression (**Fig. 6G-6I**), support CEBPB's role as a suppressive TF of *PARP1*. In addition, CEBPB
454 overexpression also conferred resistance to oxidative stress-induced cell death (**Fig. 6L**), mirroring
455 phenotypes observed in aneuploid, PARP1-downregulated, and lysosome-dysfunction cells.
456 Overall, our data establish CEBPB as a critical TF activated in aneuploid and lysosome-deficient
457 cells, suppressing PARP1 expression and contributing to oxidative stress resistance.
458

459 Discussion

460 In this study, we discovered that aneuploid cells resist ROS-induced cell death more than diploid
461 cells (**Fig. 1, 2**). Mechanistically, *PARP1* is suppressed across 15 aneuploidy models (**Fig. 2**), and
462 this suppression confers resistance to parthanatos, i.e., PARP1-mediated cell death, which can be
463 triggered by ROS, DNA alkylation, or UV radiation (**Fig. 3**). Concurrently, this suppression
464 compromises PARP1-mediated DNA damage repair in aneuploid cells (**Fig. 3**), potentially
465 contributing to cancer progression. Accordingly, we found that PARP1 levels inversely correlate
466 with metastatic potential in cancer models and human patients (**Fig. 4**). Through comprehensive
467 screening, we identified lysosomal stress and subsequent CEBPB activation as potential mediators
468 of PARP1 suppression in aneuploid cells (**Fig. 5-6**, **Fig. S6A-H**).
469

470 **Relationship between aneuploidy and ROS across different species**

471 Earlier studies in *Saccharomyces Cerevisiae* revealed that aneuploid yeasts show increased ROS
472 and hypersensitivity to H_2O_2[68], contrasting with our findings in mammalian cells. In our model,
473 aneuploid cell resistance to oxidative stress is not mediated by increased ROS-buffering capacity
474 but by reduced sensitivity to ROS-induced cell death through PARP1 suppression (**Fig. 2-3**).
475 Notably, *Saccharomyces Cerevisiae* lacks PARPs and PARP-like proteins[69], which may explain the
476 difference. Previous studies using *Drosophila* and mouse models with persistent chromosome
477 instability (CIN) reported increased intracellular ROS[70,71]. Our chromosomally stable aneuploid cells
478 showed no significant increase in ROS levels, oxidative damage, or NRF2 activation (**Fig. 2 and S2**).
479 The discrepancy may reflect species-specific effects or differences between stable aneuploidy and
480 ongoing CIN.
481

482 **PARP1 suppression in aneuploid cells is associated with CEBPB**

483 PARP1 suppression in aneuploid cells does not result from cell cycle dysregulation. PARP1
484 downregulation occurs in both *TP53*WT and *TP53*KO aneuploid cells (**Fig. 2**), despite p53-
485 dependent G1 arrest[72,73]. Additionally, aneuploid cells generated by different methods show PARP1
486 downregulation (**Fig. 2I, Fig. S2I-K**), while maintaining cell cycle profiles[74–76] and proliferation rates
487 similar to their diploid counterparts (**Fig. 1I, Fig. 4A**)

488 Our CRISPR screen identified PARP1 expression regulators, providing a valuable resource
489 for PARP1 research. Integration with RNAseq data suggested that alterations in the autophagy-
490 lysosome pathway (**Fig. S5E**), particularly lysosomal V-ATPase genes (**Fig. S5F**), may contribute
491 to PARP1 downregulation in aneuploid cells. Lysosomal stress is a common feature in aneuploid
492 cells (**Fig. 5F-H**)[29,30]. We demonstrated that lysosome inhibition induces PARP1 downregulation
493 (**Fig. 5I**), conferring cell resistance to ROS-induced cell death in a PARP1-dependent manner (**Fig.**
494 **5J-K**). These results suggest lysosomal stress is a potential mediator of PARP1 downregulation in
495 aneuploid cells.
496 Furthermore, we found that both aneuploidization and lysosome dysfunction lead to
497 increased nuclear CEBPB levels (**Fig. 6**). Genetic experiments on CEBPB support its critical role as
498 a transcriptional factor mediating PARP1 expression and ROS resistance in aneuploid cells.
499 Existing evidence supports a potential connection between aneuploidy and CEBPB, possibly via
500 proteotoxicity. Studies have demonstrated that autophagy activation or deficiency activates
501 CEBPB[77–80]. Aneuploidy is known to induce proteotoxicity, which activates autophagy through
502 transcription factor EB (TFEB)[29]. Excessive proteotoxic stress impairs autophagic flux and
503 lysosome function. Consistently, we found that further compromising autophagy through *TFEB* or
504 *TFE3* knockdown exacerbated CEBPB activation and enhanced ROS resistance in aneuploid cells,
505 while having no effect on diploid cells with intact lysosomal function. Therefore, we propose that
506 lysosome dysfunction in aneuploid cells may activate CEBPB through proteotoxicity, leading to
507 PARP1 repression and parthanatos resistance.
508
509 **PARP1 suppression and implications for cell death, DNA repair, metastasis and cancer**
510 **treatment**
511 Parthanatos, i.e. PARP1-mediated cell death, occurs after toxic insults that cause excessive
512 oxidative DNA damage[23,81] but remains poorly understood in cancer[28]. PARP1 inhibition or
513 downregulation has shown cytoprotective effects in various non-cancerous conditions[41,82–86]. Our
514 results demonstrate that modulating PARP1 levels in diploid or aneuploid cells directly affects their
515 resistance to parthanatos induced by cancer-related DNA damaging insults, such as ROS, DNA
516 alkylation, and UV radiation (**Fig. 3**). These findings may explain previous observations of
517 aneuploidy-induced resistance to certain chemotherapy and radiation therapy[10,11,87–89].
518 PARP1 downregulation also impairs repair of oxidative and alkylating DNA damage in
519 aneuploid cells (**Fig. 3M, Fig. S3J-K**), consistent with earlier research showing PARP1 depletion
520 reduces SSB repair rates[90]. Aneuploid cells did not exhibit impaired repair of DNA damage induced
521 by certain agents that may induce multiple DNA damage repair mechanisms with less dependency
522 on PARP1. The apparently paradoxical survival advantage despite impaired DNA repair may be
523 explained by PARP1's dual role: excessive PARP1 activation depletes NAD+ and ATP, which can be
524 more lethal than the DNA damage itself[26], making PARP1 suppression pro-survival under extensive
525 DNA damage. Taken together, we propose that aneuploidy may create a 'perfect storm' where

resistance to cell death is coupled with decreased DNA repair under oxidative stress via PARP1 downregulation, potentially promoting tumorigenesis and cancer evolution.

PARP1 has been an important therapeutic target for HR-deficient tumors[91]. Our findings may have implications for the clinical use of PARPi. PARP1 downregulation has been associated with PARP1i resistance[92–94], suggesting that aneuploid cancer cells may inherently resist PARP1i due to PARP1 downregulation, and analysis of CCLE cancer cell lines confirms that aneuploid cells show reduced PARPi sensitivity (**Fig. S6I**). Additionally, PARPi might counteract the cytotoxic effects of DNA damage-inducing agents if their efficacy relies on PARP1 hyperactivation and induction of parthanatos[28]. Altogether, our studies, by shedding light on a previously unappreciated effect of aneuploidy—promoting ROS resistance through PARP1 suppression—pave the way for future studies to better characterize the implications of these findings for cancer therapy and resistance.

Limitations of the Study

Several limitations should be noted. First, as intratumoral H_2O_2 concentrations are not precisely defined, our *in vitro* models may not fully recapitulate the magnitude or duration of oxidative stress during tumor progression or treatment. Second, although we demonstrate that modest PARP1 reductions alter cellular phenotypes, systematic dose-response studies are needed to precisely define cancer cell sensitivity to graded alterations in PARP1 dosage. Third, while our *in vivo* experiments link PARP1 levels to metastatic potential, it remains unclear whether this effect operates through resistance to ROS-induced parthanatos or other mechanisms. Finally, while our data establish CEBPB as a transcriptional regulator of PARP1, the precise mechanism by which aneuploidy and lysosomal dysfunction activate CEBPB specifically in aneuploid cells warrants further investigation.

STAR Methods

Summary

Aneuploidy models were generated by transient MPS1 inhibitor treatment (acute model), single-cell cloning following MPS1 inhibitor treatment (chronic model), CRISPR-mediated chromosome missegregation, or microcell-mediated chromosome transfer (MMCT). Aneuploidy was confirmed by flow cytometry and whole-genome sequencing, and aneuploidy scores were calculated from arm-level somatic copy number alterations. Cell viability was assessed by fluorescence microscopy or flow cytometry following oxidative stress or other treatments. Global RNA and protein expression were evaluated by RNA-sequencing and mass spectrometry, respectively, with gene-specific detection by RT-qPCR and western blotting. Genome-wide CRISPR knockout screening was performed with FACS-based sorting by PARP1 levels, followed by sgRNA

563 enrichment analysis using MAGeCK. PARP1, TIMELESS, CEBPB, and other genes were manipulated
564 using lentiviral shRNA knockdown, Cas9-sgRNA knockout, or cDNA overexpression. DNA damage
565 was assessed by alkaline comet assay and γH2AX staining. Metastasis was evaluated in NSG or
566 B6 Albino mice by bioluminescence imaging following cancer cell injection. Integrative analysis of
567 transcriptome and proteome data generated in this study and from published bulk and single-cell
568 RNA-sequencing datasets was used to evaluate gene expression and pathway activity. In all
569 figures, individual data points represent replicates from representative experiments (at least two
570 independent experiments were performed to validate results). For dot plots, unless otherwise
571 specified, summary statistics show mean ± standard deviation. Statistical analyses used unpaired
572 t-tests, ANOVA with post-hoc tests, or non-parametric tests as appropriate, with $p < 0.05$ considered
573 significant. Detailed methods are provided in Supplemental Information.
574
575 **Aneuploidy models**
576 *MPS1i-induced acute aneuploidy*
577 To study the short-term effects of aneuploidy, irrespective of specific chromosome gains or losses,
578 we utilized a model of **acute aneuploidy** in which near-diploid cells were treated with MPS1i
579 (reversine or AZ3146) to induce chromosome missegregation. *TP53*WT or *TP53*KO hCECs, RPE1,
580 DLD1, and mouse KP cancer cells were seeded at 30% confluency and treated with either 0.5 μM
581 reversine or 5 μM AZ3146 for 24-30 hours. hMECs were treated under similar conditions but with
582 an extended 48-hour exposure to the inhibitors. Subsequently, the cells were trypsinized and
583 cultured in the regular medium for 3 days (the release phase). Over-confluence was avoided both
584 during MPS1i treatment and the release phase. The control group was treated with an equivalent
585 amount of DMSO (0.1% v/v) for an identical duration and was then released for the same time
586 period. Both the diploid control (treated with DMSO) and the aneuploid cells (treated with reversine
587 or AZ3146) were plated on new culture dishes or plates to achieve comparable confluency on the
588 second day for downstream comparisons. To assess the potential side effects of MPS1i, confluent
589 hCECs with temporarily suppressed proliferation were treated with 0.1% DMSO or MPS1i (0.5 μM
590 reversine or 5 μM AZ3146) for 24-30 hours, followed by a 3-day release and replating for
591 downstream experiments. Over-confluence was only avoided during the release phase. The
592 induction of aneuploidy was confirmed through flow cytometric analysis of DNA content and
593 scRNAseq-based CNA quantification (see description below).
594
595 *Isogenic clones containing different aneuploidy levels*
596 To study the longer-term effects during adaptive stages of aneuploidy, irrespective of specific
597 chromosome gains or losses, a model of **chronic aneuploidy** was developed. Near-diploid *TP53*KO
598 hCECs were exposed to 0.2 μM reversine for 24 hours. Then they were plated at a low density and
599 allowed to grow until colonies formed. Single-cell-derived clones were isolated using glass
600 cylinders and transferred to separate wells in multiwell plates for further expansion. To identify

601 chromosomal gains and losses, the DNA of a cohort of 56 isogenic hCEC clones was extracted and
602 subjected to shallow whole-genome sequencing (see description below). The clones were
603 categorized as near-diploid, exhibiting 0-2 gains or losses of chromosomes or chromosome arms
604 (designated as D followed by numbers), or as aneuploid, with ≥ 5 gains or losses of chromosomes
605 or chromosome arms (designated as A followed by numbers). The clones maintained stable
606 karyotypes over one month of *in vitro* culture.
607
608 *Previously published Aneuploidy models generated by MMCT*
609 Microcell-mediated chromosome transfer (MMCT) is a common method for generating aneuploid
610 clones with one or two extra chromosomes[95]. Aneuploid clones of HCT116 with an extra
611 chromosome 5 and RPE1 with an extra chromosome 7, along with their diploid control clones[32],
612 generously provided by Dr. Zuzana Storchová and Dr. Jason M. Sheltzer, served as an independent
613 aneuploidy model to test our hypotheses.
614
615 **Aneuploidy score**
616 Aneuploidy was quantified by estimating the total number of arm-level gains and losses for each
617 hCEC clone, cancer cell line, or tumor sample. For hCEC clones, the arm-level copy number
618 alterations were calculated based on the copy number package[96]. We considered a log2-
619 transformed copy number ratio > 0.3 as a gain and < (−0.3) as a loss. The aneuploidy scores of
620 CCLE cancer cell lines were downloaded from Depmap portal[97]. For Fig. 4B and 4C, cell lines were
621 stratified into three groups based on aneuploid scores (low, medium, and high aneuploidy) with the
622 same number of cells in each group (pan-cancer: 314 cell lines per group; COREAD: 18 cell lines per
623 group). For TCGA COREAD samples, the arm and gene level somatic copy number alteration data
624 were obtained from the TCGA dataset. The log2-transformed copy number ratios for each
625 chromosomal region were adjusted by tumor purity and ploidy using ABSOLUTE method [98].
626 Sample-related purity and ploidy were downloaded from TCGA Firehose Legacy. The detailed
627 method for copy number adjustment based on purity and ploidy was described before[99]. After the
628 adjustment, we considered a log2-transformed copy number ratio > 0.3 as a gain and < (−0.3) as a
629 loss.
630
631

632 # References

633 1. Weaver, B.A., and Cleveland, D.W. (2008). The aneuploidy paradox in cell growth and
634 tumorigenesis. Cancer Cell *14*, 431–433. https://doi.org/10.1016/j.ccr.2008.11.011.

635 2. Ben-David, U., and Amon, A. (2020). Context is everything: aneuploidy in cancer. Nat.
636 Rev. Genet. *21*, 44–62. https://doi.org/10.1038/s41576-019-0171-x.

637 3. Knouse, K.A., Davoli, T., Elledge, S.J., and Amon, A. (2017). Aneuploidy in Cancer: Seq-
638 ing Answers to Old Questions. Annu. Rev. Cancer Biol. *1*, 335–354.
639 https://doi.org/10.1146/annurev-cancerbio-042616-072231.

640 4. Lukow, D.A., and Sheltzer, J.M. (2021). Chromosomal instability and aneuploidy as causes
641 of cancer drug resistance. Trends Cancer. https://doi.org/10.1016/j.trecan.2021.09.002.

642 5. Davoli, T., Xu, A.W., Mengwasser, K.E., Sack, L.M., Yoon, J.C., Park, P.J., and Elledge,
643 S.J. (2013). Cumulative haploinsufficiency and triplosensitivity drive aneuploidy patterns
644 and shape the cancer genome. Cell *155*, 948–962.
645 https://doi.org/10.1016/j.cell.2013.10.011.

646 6. William, W.N., Zhao, X., Bianchi, J.J., Lin, H.Y., Cheng, P., Lee, J.J., Carter, H.,
647 Alexandrov, L.B., Abraham, J.P., Spetzler, D.B., et al. (2021). Immune evasion in HPV-
648 head and neck precancer-cancer transition is driven by an aneuploid switch involving
649 chromosome 9p loss. Proc. Natl. Acad. Sci. U. S. A. *118*, e2022655118.
650 https://doi.org/10.1073/pnas.2022655118.

651 7. Cheng, P., Singh, K., Reeves, R.H., and Davoli, T. (2025). The Hallmarks of Aneuploidy in
652 Cancer and Congenital Syndromes. Annu. Rev. Genomics Hum. Genet. *26*, 103–138.
653 https://doi.org/10.1146/annurev-genom-111723-103557.

654 8. Santaguida, S., and Amon, A. (2015). Short- and long-term effects of chromosome mis-
655 segregation and aneuploidy. Nat. Rev. Mol. Cell Biol. *16*, 473–485.
656 https://doi.org/10.1038/nrm4025.

657 9. Zhu, J., Tsai, H.-J., Gordon, M.R., and Li, R. (2018). Cellular Stress Associated with
658 Aneuploidy. Dev. Cell *44*, 420–431. https://doi.org/10.1016/j.devcel.2018.02.002.

659 10. Replogle, J.M., Zhou, W., Amaro, A.E., McFarland, J.M., Villalobos-Ortiz, M., Ryan, J.,
660 Letai, A., Yilmaz, O., Sheltzer, J., Lippard, S.J., et al. (2020). Aneuploidy increases
661 resistance to chemotherapeutics by antagonizing cell division. Proc. Natl. Acad. Sci. *117*,
662 30566–30576. https://doi.org/10.1073/pnas.2009506117.

663 11. Zerbib, J., Ippolito, M.R., Eliezer, Y., De Feudis, G., Reuveni, E., Savir Kadmon, A., Martin,
664 S., Viganò, S., Leor, G., Berstler, J., et al. (2024). Human aneuploid cells depend on the
665 RAF/MEK/ERK pathway for overcoming increased DNA damage. Nat. Commun. *15*, 7772.
666 https://doi.org/10.1038/s41467-024-52176-x.

667 12. Taylor, A.M., Shih, J., Ha, G., Gao, G.F., Zhang, X., Berger, A.C., Schumacher, S.E.,
668 Wang, C., Hu, H., Liu, J., et al. (2018). Genomic and Functional Approaches to

669 Understanding Cancer Aneuploidy. Cancer Cell *33*, 676-689.e3.
670 https://doi.org/10.1016/j.ccell.2018.03.007.

671 13. Girish, V., Lakhani, A.A., Thompson, S.L., Scaduto, C.M., Brown, L.M., Hagenson, R.A.,
672 Sausville, E.L., Mendelson, B.E., Kandikuppa, P.K., Lukow, D.A., et al. (2023). Oncogene-
673 like addiction to aneuploidy in human cancers. Science *381*, eadg4521.
674 https://doi.org/10.1126/science.adg4521.

675 14. Shih, J., Sarmashghi, S., Zhakula-Kostadinova, N., Zhang, S., Georgis, Y., Hoyt, S.H.,
676 Cuoco, M.S., Gao, G.F., Spurr, L.F., Berger, A.C., et al. (2023). Cancer aneuploidies are
677 shaped primarily by effects on tumour fitness. Nature *619*, 793–800.
678 https://doi.org/10.1038/s41586-023-06266-3.

679 15. Reczek, C.R., and Chandel, N.S. (2017). The Two Faces of Reactive Oxygen Species in
680 Cancer. Annu. Rev. Cancer Biol. *1*, 79–98. https://doi.org/10.1146/annurev-cancerbio-
681 041916-065808.

682 16. Gorrini, C., Harris, I.S., and Mak, T.W. (2013). Modulation of oxidative stress as an
683 anticancer strategy. Nat. Rev. Drug Discov. *12*, 931–947. https://doi.org/10.1038/nrd4002.

684 17. Hayes, J.D., Dinkova-Kostova, A.T., and Tew, K.D. (2020). Oxidative Stress in Cancer.
685 Cancer Cell *38*, 167–197. https://doi.org/10.1016/j.ccell.2020.06.001.

686 18. Piskounova, E., Agathocleous, M., Murphy, M.M., Hu, Z., Huddlestun, S.E., Zhao, Z.,
687 Leitch, A.M., Johnson, T.M., DeBerardinis, R.J., and Morrison, S.J. (2015). Oxidative
688 stress inhibits distant metastasis by human melanoma cells. Nature *527*, 186–191.
689 https://doi.org/10.1038/nature15726.

690 19. Crist, S.B., Nemkov, T., Dumpit, R.F., Dai, J., Tapscott, S.J., True, L.D., Swarbrick, A.,
691 Sullivan, L.B., Nelson, P.S., Hansen, K.C., et al. (2022). Unchecked oxidative stress in
692 skeletal muscle prevents outgrowth of disseminated tumour cells. Nat. Cell Biol. *24*, 538–
693 553. https://doi.org/10.1038/s41556-022-00881-4.

694 20. Nguyen, B., Fong, C., Luthra, A., Smith, S.A., DiNatale, R.G., Nandakumar, S., Walch, H.,
695 Chatila, W.K., Madupuri, R., Kundra, R., et al. (2022). Genomic characterization of
696 metastatic patterns from prospective clinical sequencing of 25,000 patients. Cell *185*, 563-
697 575.e11. https://doi.org/10.1016/j.cell.2022.01.003.

698 21. Caldecott, K.W. (2008). Single-strand break repair and genetic disease. Nat. Rev. Genet.
699 *9*, 619–631. https://doi.org/10.1038/nrg2380.

700 22. Ray Chaudhuri, A., and Nussenzweig, A. (2017). The multifaceted roles of PARP1 in DNA
701 repair and chromatin remodelling. Nat. Rev. Mol. Cell Biol. *18*, 610–621.
702 https://doi.org/10.1038/nrm.2017.53.

703 23. David, K.K., Andrabi, S.A., Dawson, T.M., and Dawson, V.L. (2009). Parthanatos, a
704 messenger of death. Front. Biosci. Landmark Ed. *14*, 1116–1128.

705 24. Ha, H.C., and Snyder, S.H. (1999). Poly(ADP-ribose) polymerase is a mediator of necrotic
706 cell death by ATP depletion. Proc. Natl. Acad. Sci. *96*, 13978–13982.
707 https://doi.org/10.1073/pnas.96.24.13978.

25. Andrabi, S.A., Dawson, T.M., and Dawson, V.L. (2008). Mitochondrial and Nuclear Cross Talk in Cell Death. Ann. N. Y. Acad. Sci. *1147*, 233–241. https://doi.org/10.1196/annals.1427.014.

26. Roos, W.P., Thomas, A.D., and Kaina, B. (2016). DNA damage and the balance between survival and death in cancer biology. Nat. Rev. Cancer *16*, 20–33. https://doi.org/10.1038/nrc.2015.2.

27. Eliasson, M.J., Sampei, K., Mandir, A.S., Hurn, P.D., Traystman, R.J., Bao, J., Pieper, A., Wang, Z.Q., Dawson, T.M., Snyder, S.H., et al. (1997). Poly(ADP-ribose) polymerase gene disruption renders mice resistant to cerebral ischemia. Nat. Med. *3*, 1089–1095. https://doi.org/10.1038/nm1097-1089.

28. Maru, B., Messikommer, A., Huang, L., Seipel, K., Kovecses, O., Valk, P.J.M., Theocharides, A.P.A., Mercier, F.E., Pabst, T., McKeague, M., et al. (2023). PARP-1 improves leukemia outcomes by inducing parthanatos during chemotherapy. Cell Rep. Med. *4*, 101191. https://doi.org/10.1016/j.xcrm.2023.101191.

29. Santaguida, S., Vasile, E., White, E., and Amon, A. (2015). Aneuploidy-induced cellular stresses limit autophagic degradation. Genes Dev. *29*, 2010–2021. https://doi.org/10.1101/gad.269118.115.

30. Dürrbaum, M., Kuznetsova, A.Y., Passerini, V., Stingele, S., Stoehr, G., and Storchová, Z. (2014). Unique features of the transcriptional response to model aneuploidy in human cells. BMC Genomics *15*, 139. https://doi.org/10.1186/1471-2164-15-139.

31. Cheng, P., Zhao, X., Katsnelson, L., Camacho-Hernandez, E.M., Mermerian, A., Mays, J.C., Lippman, S.M., Rosales-Alvarez, R.E., Moya, R., Shwetar, J., et al. (2022). Proteogenomic analysis of cancer aneuploidy and normal tissues reveals divergent modes of gene regulation across cellular pathways. eLife *11*, e75227. https://doi.org/10.7554/eLife.75227.

32. Stingele, S., Stoehr, G., Peplowska, K., Cox, J., Mann, M., and Storchova, Z. (2012). Global analysis of genome, transcriptome and proteome reveals the response to aneuploidy in human cells. Mol. Syst. Biol. *8*, 608. https://doi.org/10.1038/msb.2012.40.

33. Liu, Y., Marks, K., Cowley, G.S., Carretero, J., Liu, Q., Nieland, T.J.F., Xu, C., Cohoon, T.J., Gao, P., Zhang, Y., et al. (2013). Metabolic and functional genomic studies identify deoxythymidylate kinase as a target in LKB1-mutant lung cancer. Cancer Discov. *3*, 870–879. https://doi.org/10.1158/2159-8290.CD-13-0015.

34. Chen, Z., Cheng, K., Walton, Z., Wang, Y., Ebi, H., Shimamura, T., Liu, Y., Tupper, T., Ouyang, J., Li, J., et al. (2012). A murine lung cancer co-clinical trial identifies genetic modifiers of therapeutic response. Nature *483*, 613–617. https://doi.org/10.1038/nature10937.

35. Jacobi, J., Kristal, B., Chezar, J., Shaul, S.M., and Sela, S. (2005). Exogenous superoxide mediates pro-oxidative, proinflammatory, and procoagulatory changes in primary endothelial cell cultures. Free Radic. Biol. Med. *39*, 1238–1248. https://doi.org/10.1016/j.freeradbiomed.2005.06.010.

36. Ma, Q. (2013). Role of Nrf2 in Oxidative Stress and Toxicity. Annu. Rev. Pharmacol. Toxicol. *53*, 401–426. https://doi.org/10.1146/annurev-pharmtox-011112-140320.

37. Hirakata, C., Lima, K., De Almeida, B.O., De Miranda, L.B.L., Florêncio, K.G.D., Furtado, L.C., Costa-Lotufo, L.V., and Machado-Neto, J.A. (2021). Targeting glioma cells by antineoplastic activity of reversine. Oncol. Lett. *22*, 610. https://doi.org/10.3892/ol.2021.12871.

38. Sanchez-Vasquez, E., Bronner, M.E., and Zernicka-Goetz, M. (2023). HIF1A contributes to the survival of aneuploid and mosaic pre-implantation embryos. Preprint at bioRxiv, https://doi.org/10.1101/2023.09.04.556218 https://doi.org/10.1101/2023.09.04.556218.

39. Kaufmann, S.H., Desnoyers, S., Ottaviano, Y., Davidson, N.E., and Poirier, G.G. (1993). Specific Proteolytic Cleavage of Poly(ADP-ribose) Polymerase: An Early Marker of Chemotherapy-induced Apoptosis1. Cancer Res. *53*, 3976–3985.

40. Wang, X., Liu, L., Montagna, C., Ried, T., and Deng, C.-X. (2007). Haploinsufficiency of Parp1 accelerates Brca1-associated centrosome amplification, telomere shortening, genetic instability, apoptosis, and embryonic lethality. Cell Death Differ. *14*, 924–931. https://doi.org/10.1038/sj.cdd.4402105.

41. Fatokun, A.A., Dawson, V.L., and Dawson, T.M. (2014). Parthanatos: mitochondrial-linked mechanisms and therapeutic opportunities. Br. J. Pharmacol. *171*, 2000–2016. https://doi.org/10.1111/bph.12416.

42. Young, L.M., Marzio, A., Perez-Duran, P., Reid, D.A., Meredith, D.N., Roberti, D., Star, A., Rothenberg, E., Ueberheide, B., and Pagano, M. (2015). TIMELESS Forms a Complex with PARP1 Distinct from Its Complex with TIPIN and Plays a Role in the DNA Damage Response. Cell Rep. *13*, 451–459. https://doi.org/10.1016/j.celrep.2015.09.017.

43. Amé, J.C., Rolli, V., Schreiber, V., Niedergang, C., Apiou, F., Decker, P., Muller, S., Höger, T., Ménissier-de Murcia, J., and de Murcia, G. (1999). PARP-2, A novel mammalian DNA damage-dependent poly(ADP-ribose) polymerase. J. Biol. Chem. *274*, 17860–17868. https://doi.org/10.1074/jbc.274.25.17860.

44. Wang, Y., An, R., Umanah, G.K., Park, H., Nambiar, K., Eacker, S.M., Kim, B., Bao, L., Harraz, M.M., Chang, C., et al. (2016). A nuclease that mediates cell death induced by DNA damage and poly(ADP-ribose) polymerase-1. Science *354*, aad6872. https://doi.org/10.1126/science.aad6872.

45. Hurtado-Bagès, S., Knobloch, G., Ladurner, A.G., and Buschbeck, M. (2020). The taming of PARP1 and its impact on NAD+ metabolism. Mol. Metab. *38*, 100950. https://doi.org/10.1016/j.molmet.2020.01.014.

46. Ciccia, A., and Elledge, S.J. (2010). The DNA Damage Response: Making It Safe to Play with Knives. Mol. Cell *40*, 179–204. https://doi.org/10.1016/j.molcel.2010.09.019.

47. Artus, C., Boujrad, H., Bouharrour, A., Brunelle, M.-N., Hoos, S., Yuste, V.J., Lenormand, P., Rousselle, J.-C., Namane, A., England, P., et al. (2010). AIF promotes chromatinolysis and caspase-independent programmed necrosis by interacting with histone H2AX. EMBO J. *29*, 1585–1599. https://doi.org/10.1038/emboj.2010.43.

48. Sayin, V.I., Ibrahim, M.X., Larsson, E., Nilsson, J.A., Lindahl, P., and Bergo, M.O. (2014). Antioxidants accelerate lung cancer progression in mice. Sci. Transl. Med. *6*, 221ra15. https://doi.org/10.1126/scitranslmed.3007653.

49. Cancer Genome Atlas Research Network, Weinstein, J.N., Collisson, E.A., Mills, G.B., Shaw, K.R.M., Ozenberger, B.A., Ellrott, K., Shmulevich, I., Sander, C., and Stuart, J.M. (2013). The Cancer Genome Atlas Pan-Cancer analysis project. Nat. Genet. *45*, 1113–1120. https://doi.org/10.1038/ng.2764.

50. Laubert, T., Freitag-Wolf, S., Linnebacher, M., König, A., Vollmar, B., Habermann, J.K., and on behalf of the North German Tumorbank of Colorectal Cancer (ColoNet) consortium (2015). Stage-specific frequency and prognostic significance of aneuploidy in patients with sporadic colorectal cancer—a meta-analysis and current overview. Int. J. Colorectal Dis. *30*, 1015–1028. https://doi.org/10.1007/s00384-015-2259-x.

51. Dörsam, B., Seiwert, N., Foersch, S., Stroh, S., Nagel, G., Begaliew, D., Diehl, E., Kraus, A., McKeague, M., Minneker, V., et al. (2018). PARP-1 protects against colorectal tumor induction, but promotes inflammation-driven colorectal tumor progression. Proc. Natl. Acad. Sci. *115*, E4061–E4070. https://doi.org/10.1073/pnas.1712345115.

52. Kamal, Y., Schmit, S.L., Hoehn, H.J., Amos, C.I., and Frost, H.R. (2019). Transcriptomic Differences between Primary Colorectal Adenocarcinomas and Distant Metastases Reveal Metastatic Colorectal Cancer Subtypes. Cancer Res. *79*, 4227–4241. https://doi.org/10.1158/0008-5472.CAN-18-3945.

53. Zhu, X., Zhang, H., and Mendell, J.T. (2020). Ribosome Recycling by ABCE1 Links Lysosomal Function and Iron Homeostasis to 3' UTR-Directed Regulation and Nonsense-Mediated Decay. Cell Rep. *32*, 107895. https://doi.org/10.1016/j.celrep.2020.107895.

54. Weber, R.A., Yen, F.S., Nicholson, S.P.V., Alwaseem, H., Bayraktar, E.C., Alam, M., Timson, R.C., La, K., Abu-Remaileh, M., Molina, H., et al. (2020). Maintaining Iron Homeostasis Is the Key Role of Lysosomal Acidity for Cell Proliferation. Mol. Cell *77*, 645-655.e7. https://doi.org/10.1016/j.molcel.2020.01.003.

55. S, S., I, Z., Jk, D.B., and Mg, R. (2010). Inhibition of iron uptake is responsible for differential sensitivity to V-ATPase inhibitors in several cancer cell lines. PloS One *5*. https://doi.org/10.1371/journal.pone.0011629.

56. Wu, T., Wang, G., Chen, W., Zhu, Z., Liu, Y., Huang, Z., Huang, Y., Du, P., Yang, Y., Liu, C.-Y., et al. (2018). Co-inhibition of BET proteins and NF-κB as a potential therapy for colorectal cancer through synergistic inhibiting MYC and FOXM1 expressions. Cell Death Dis. *9*, 315. https://doi.org/10.1038/s41419-018-0354-y.

57. Tu, C., Liu, Y., Williams, D.R., and Wu, J.C. (2022). A transcriptomic atlas of drug-induced endothelial dysfunction in human endothelial cells. J. Mol. Cell. Cardiol. *173*, 115–117. https://doi.org/10.1016/j.yjmcc.2022.10.002.

58. Cáceres-Gutiérrez, R.E., Andonegui, M.A., Oliva-Rico, D.A., González-Barrios, R., Luna, F., Arriaga-Canon, C., López-Saavedra, A., Prada, D., Castro, C., Parmentier, L., et al. (2022). Proteasome inhibition alters mitotic progression through the upregulation of centromeric α-Satellite RNAs. FEBS J. *289*, 1858–1875.

https://doi.org/10.1111/febs.16261.

59. Shen, W.-K., Chen, S.-Y., Gan, Z.-Q., Zhang, Y.-Z., Yue, T., Chen, M.-M., Xue, Y., Hu, H., and Guo, A.-Y. (2023). AnimalTFDB 4.0: a comprehensive animal transcription factor database updated with variation and expression annotations. Nucleic Acids Res. *51*, D39–D45. https://doi.org/10.1093/nar/gkac907.

60. Liska, O., Bohár, B., Hidas, A., Korcsmáros, T., Papp, B., Fazekas, D., and Ari, E. (2022). TFLink: an integrated gateway to access transcription factor-target gene interactions for multiple species. Database J. Biol. Databases Curation *2022*, baac083. https://doi.org/10.1093/database/baac083.

61. Fishilevich, S., Nudel, R., Rappaport, N., Hadar, R., Plaschkes, I., Iny Stein, T., Rosen, N., Kohn, A., Twik, M., Safran, M., et al. (2017). GeneHancer: genome-wide integration of enhancers and target genes in GeneCards. Database J. Biol. Databases Curation *2017*, bax028. https://doi.org/10.1093/database/bax028.

62. Hitz, B.C., Jin-Wook, L., Jolanki, O., Kagda, M.S., Graham, K., Sud, P., Gabdank, I., Strattan, J.S., Sloan, C.A., Dreszer, T., et al. (2023). The ENCODE Uniform Analysis Pipelines. BioRxiv Prepr. Serv. Biol., 2023.04.04.535623. https://doi.org/10.1101/2023.04.04.535623.

63. Keenan, A.B., Torre, D., Lachmann, A., Leong, A.K., Wojciechowicz, M.L., Utti, V., Jagodnik, K.M., Kropiwnicki, E., Wang, Z., and Ma'ayan, A. (2019). ChEA3: transcription factor enrichment analysis by orthogonal omics integration. Nucleic Acids Res. *47*, W212–W224. https://doi.org/10.1093/nar/gkz446.

64. Settembre, C., Di Malta, C., Polito, V.A., Garcia Arencibia, M., Vetrini, F., Erdin, S., Erdin, S.U., Huynh, T., Medina, D., Colella, P., et al. (2011). TFEB links autophagy to lysosomal biogenesis. Science *332*, 1429–1433. https://doi.org/10.1126/science.1204592.

65. Southard, K.M., Ardy, R.C., Tang, A., O'Sullivan, D.D., Metzner, E., Guruvayurappan, K., and Norman, T.M. (2024). Comprehensive transcription factor perturbations recapitulate fibroblast transcriptional states. Preprint at bioRxiv, https://doi.org/10.1101/2024.07.31.606073 https://doi.org/10.1101/2024.07.31.606073.

66. Tyler, M., Gavish, A., Barbolin, C., Tschernichovsky, R., Hoefflin, R., Mints, M., Puram, S.V., and Tirosh, I. (2024). The Curated Cancer Cell Atlas: comprehensive characterisation of tumours at single-cell resolution. Preprint at bioRxiv, https://doi.org/10.1101/2024.10.11.617836 https://doi.org/10.1101/2024.10.11.617836.

67. Pelka, K., Hofree, M., Chen, J.H., Sarkizova, S., Pirl, J.D., Jorgji, V., Bejnood, A., Dionne, D., Ge, W.H., Xu, K.H., et al. (2021). Spatially organized multicellular immune hubs in human colorectal cancer. Cell *184*, 4734-4752.e20. https://doi.org/10.1016/j.cell.2021.08.003.

68. Dephoure, N., Hwang, S., O'Sullivan, C., Dodgson, S.E., Gygi, S.P., Amon, A., and Torres, E.M. (2014). Quantitative proteomic analysis reveals posttranslational responses to aneuploidy in yeast. eLife *3*, e03023. https://doi.org/10.7554/eLife.03023.

69. Citarelli, M., Teotia, S., and Lamb, R.S. (2010). Evolutionary history of the poly(ADP-

869 ribose) polymerase gene family in eukaryotes. BMC Evol. Biol. *10*, 308.
870 https://doi.org/10.1186/1471-2148-10-308.

871 70. Clemente-Ruiz, M., Murillo-Maldonado, J.M., Benhra, N., Barrio, L., Pérez, L., Quiroga, G.,
872 Nebreda, A.R., and Milán, M. (2016). Gene Dosage Imbalance Contributes to
873 Chromosomal Instability-Induced Tumorigenesis. Dev. Cell *36*, 290–302.
874 https://doi.org/10.1016/j.devcel.2016.01.008.

875 71. Li, M., Fang, X., Baker, D.J., Guo, L., Gao, X., Wei, Z., Han, S., van Deursen, J.M., and
876 Zhang, P. (2010). The ATM-p53 pathway suppresses aneuploidy-induced tumorigenesis.
877 Proc. Natl. Acad. Sci. U. S. A. *107*, 14188–14193.
878 https://doi.org/10.1073/pnas.1005960107.

879 72. Thompson, S.L., and Compton, D.A. (2010). Proliferation of aneuploid human cells is
880 limited by a p53-dependent mechanism. J. Cell Biol. *188*, 369–381.
881 https://doi.org/10.1083/jcb.200905057.

882 73. Santaguida, S., Richardson, A., Iyer, D.R., M'Saad, O., Zasadil, L., Knouse, K.A., Wong,
883 Y.L., Rhind, N., Desai, A., and Amon, A. (2017). Chromosome Mis-segregation Generates
884 Cell-Cycle-Arrested Cells with Complex Karyotypes that Are Eliminated by the Immune
885 System. Dev. Cell *41*, 638-651.e5. https://doi.org/10.1016/j.devcel.2017.05.022.

886 74. Passerini, V., Ozeri-Galai, E., de Pagter, M.S., Donnelly, N., Schmalbrock, S.,
887 Kloosterman, W.P., Kerem, B., and Storchová, Z. (2016). The presence of extra
888 chromosomes leads to genomic instability. Nat. Commun. *7*, 10754.
889 https://doi.org/10.1038/ncomms10754.

890 75. Jacob, S., Aguado, M., Fallik, D., and Praz, F. (2001). The Role of the DNA Mismatch
891 Repair System in the Cytotoxicity of the Topoisomerase Inhibitors Camptothecin and
892 Etoposide to Human Colorectal Cancer Cells1. Cancer Res. *61*, 6555–6562.

893 76. Bazzocco, S., Dopeso, H., Carton-Garcia, F., Macaya, I., Andretta, E., Chionh, F.,
894 Rodrigues, P., Garrido, M., Alazzouzi, H., Nieto, R., et al. (2015). Highly Expressed Genes
895 in Rapidly Proliferating Tumor Cells as New Targets for Colorectal Cancer Treatment. Clin.
896 Cancer Res. *21*, 3695–3704. https://doi.org/10.1158/1078-0432.CCR-14-2457.

897 77. Zhu, Y., Liu, Y., Ma, Y., Chen, L., Huang, H., Huang, S., Zhang, H., He, Y., Tan, C., He, Y.,
898 et al. (2023). Macrophage autophagy deficiency-induced CEBPB accumulation alleviates
899 atopic dermatitis via impairing M2 polarization. Cell Rep. *42*, 113430.
900 https://doi.org/10.1016/j.celrep.2023.113430.

901 78. Kim, D., Kim, J., Yu, Y.S., Kim, Y.R., Baek, S.H., and Won, K.-J. (2022). Systemic
902 approaches using single cell transcriptome reveal that C/EBPγ regulates autophagy under
903 amino acid starved condition. Nucleic Acids Res. *50*, 7298–7309.
904 https://doi.org/10.1093/nar/gkac593.

905 79. Podust, L.M., Krezel, A.M., and Kim, Y. (2001). Crystal Structure of the CCAAT
906 Box/Enhancer-binding Protein β Activating Transcription Factor-4 Basic Leucine Zipper
907 Heterodimer in the Absence of DNA*. J. Biol. Chem. *276*, 505–513.
908 https://doi.org/10.1074/jbc.M005594200.

80. Wadgaonkar, P., Bi, Z., Wan, J., Fu, Y., Zhang, Q., Almutairy, B., Zhang, W., Qiu, Y., Thakur, C., Hüttemann, M., et al. (2022). Arsenic Activates the ER Stress-Associated Unfolded Protein Response via the Activating Transcription Factor 6 in Human Bronchial Epithelial Cells. Biomedicines *10*, 967. https://doi.org/10.3390/biomedicines10050967.

81. Pacher, P., and Szabo, C. (2008). Role of the peroxynitrite-poly(ADP-ribose) polymerase pathway in human disease. Am. J. Pathol. *173*, 2–13. https://doi.org/10.2353/ajpath.2008.080019.

82. Nassour, J., Martien, S., Martin, N., Deruy, E., Tomellini, E., Malaquin, N., Bouali, F., Sabatier, L., Wernert, N., Pinte, S., et al. (2016). Defective DNA single-strand break repair is responsible for senescence and neoplastic escape of epithelial cells. Nat. Commun. *7*, 10399. https://doi.org/10.1038/ncomms10399.

83. Oláh, G., Szczesny, B., Brunyánszki, A., López-García, I.A., Gerö, D., Radák, Z., and Szabo, C. (2015). Differentiation-Associated Downregulation of Poly(ADP-Ribose) Polymerase-1 Expression in Myoblasts Serves to Increase Their Resistance to Oxidative Stress. PLOS ONE *10*, e0134227. https://doi.org/10.1371/journal.pone.0134227.

84. Yu, S.-W., Wang, H., Poitras, M.F., Coombs, C., Bowers, W.J., Federoff, H.J., Poirier, G.G., Dawson, T.M., and Dawson, V.L. (2002). Mediation of Poly(ADP-Ribose) Polymerase-1-Dependent Cell Death by Apoptosis-Inducing Factor. Science *297*, 259–263. https://doi.org/10.1126/science.1072221.

85. Dawson, T.M., and Dawson, V.L. (2017). Mitochondrial Mechanisms of Neuronal Cell Death: Potential Therapeutics. Annu. Rev. Pharmacol. Toxicol. *57*, 437–454. https://doi.org/10.1146/annurev-pharmtox-010716-105001.

86. Zheng, J., Devalaraja-Narashimha, K., Singaravelu, K., and Padanilam, B.J. (2005). Poly(ADP-ribose) polymerase-1 gene ablation protects mice from ischemic renal injury. Am. J. Physiol.-Ren. Physiol. *288*, F387–F398. https://doi.org/10.1152/ajprenal.00436.2003.

87. Lukow, D.A., Sausville, E.L., Suri, P., Chunduri, N.K., Wieland, A., Leu, J., Smith, J.C., Girish, V., Kumar, A.A., Kendall, J., et al. (2021). Chromosomal instability accelerates the evolution of resistance to anti-cancer therapies. Dev. Cell *56*, 2427-2439.e4. https://doi.org/10.1016/j.devcel.2021.07.009.

88. Ippolito, M.R., Martis, V., Martin, S., Tijhuis, A.E., Hong, C., Wardenaar, R., Dumont, M., Zerbib, J., Spierings, D.C.J., Fachinetti, D., et al. (2021). Gene copy-number changes and chromosomal instability induced by aneuploidy confer resistance to chemotherapy. Dev. Cell *56*, 2440-2454.e6. https://doi.org/10.1016/j.devcel.2021.07.006.

89. Lee, A.J.X., Endesfelder, D., Rowan, A.J., Walther, A., Birkbak, N.J., Futreal, P.A., Downward, J., Szallasi, Z., Tomlinson, I.P.M., Howell, M., et al. (2011). Chromosomal instability confers intrinsic multidrug resistance. Cancer Res. *71*, 1858–1870. https://doi.org/10.1158/0008-5472.CAN-10-3604.

90. Fisher, A.E.O., Hochegger, H., Takeda, S., and Caldecott, K.W. (2007). Poly(ADP-Ribose) Polymerase 1 Accelerates Single-Strand Break Repair in Concert with Poly(ADP-Ribose) Glycohydrolase. Mol. Cell. Biol. *27*, 5597–5605. https://doi.org/10.1128/MCB.02248-06.

950 91. Lord, C.J., and Ashworth, A. (2017). PARP Inhibitors: The First Synthetic Lethal Targeted
951 Therapy. Science *355*, 1152–1158. https://doi.org/10.1126/science.aam7344.

952 92. Murai, J., Huang, S.N., Das, B.B., Renaud, A., Zhang, Y., Doroshow, J.H., Ji, J., Takeda,
953 S., and Pommier, Y. (2012). Trapping of PARP1 and PARP2 by Clinical PARP Inhibitors.
954 Cancer Res. *72*, 5588–5599. https://doi.org/10.1158/0008-5472.CAN-12-2753.

955 93. Byers, L.A., Wang, J., Nilsson, M.B., Fujimoto, J., Saintigny, P., Yordy, J., Giri, U., Peyton,
956 M., Fan, Y.H., Diao, L., et al. (2012). Proteomic Profiling Identifies Dysregulated Pathways
957 in Small Cell Lung Cancer and Novel Therapeutic Targets Including PARP1. Cancer
958 Discov. *2*, 798–811. https://doi.org/10.1158/2159-8290.CD-12-0112.

959 94. França, G.S., Baron, M., King, B.R., Bossowski, J.P., Bjornberg, A., Pour, M., Rao, A.,
960 Patel, A.S., Misirlioglu, S., Barkley, D., et al. (2024). Cellular adaptation to cancer therapy
961 along a resistance continuum. Nature *631*, 876–883. https://doi.org/10.1038/s41586-024-
962 07690-9.

963 95. Chunduri, N.K., and Storchová, Z. (2019). The diverse consequences of aneuploidy. Nat.
964 Cell Biol. *21*, 54–62. https://doi.org/10.1038/s41556-018-0243-8.

965 96. Nilsen, G., Liestøl, K., Van Loo, P., Moen Vollan, H.K., Eide, M.B., Rueda, O.M., Chin, S.-
966 F., Russell, R., Baumbusch, L.O., Caldas, C., et al. (2012). Copynumber: Efficient
967 algorithms for single- and multi-track copy number segmentation. BMC Genomics *13*, 591.
968 https://doi.org/10.1186/1471-2164-13-591.

969 97. Cohen-Sharir, Y., McFarland, J.M., Abdusamad, M., Marquis, C., Bernhard, S.V.,
970 Kazachkova, M., Tang, H., Ippolito, M.R., Laue, K., Zerbib, J., et al. (2021). Aneuploidy
971 renders cancer cells vulnerable to mitotic checkpoint inhibition. Nature *590*, 486–491.
972 https://doi.org/10.1038/s41586-020-03114-6.

973 98. Carter, S.L., Cibulskis, K., Helman, E., McKenna, A., Shen, H., Zack, T., Laird, P.W.,
974 Onofrio, R.C., Winckler, W., Weir, B.A., et al. (2012). Absolute quantification of somatic
975 DNA alterations in human cancer. Nat. Biotechnol. *30*, 413–421.
976 https://doi.org/10.1038/nbt.2203.

977 99. Zhao, X., Cohen, E.E.W., William, W.N., Bianchi, J.J., Abraham, J.P., Magee, D., Spetzler,
978 D.B., Gutkind, J.S., Alexandrov, L.B., Cavenee, W.K., et al. (2022). Somatic 9p24.1
979 alterations in HPV- head and neck squamous cancer dictate immune microenvironment
980 and anti-PD-1 checkpoint inhibitor activity. Proc. Natl. Acad. Sci. U. S. A. *119*,
981 e2213835119. https://doi.org/10.1073/pnas.2213835119.

982 100. Roig, A.I., Eskiocak, U., Hight, S.K., Kim, S.B., Delgado, O., Souza, R.F., Spechler, S.J.,
983 Wright, W.E., and Shay, J.W. (2010). Immortalized Epithelial Cells Derived From Human
984 Colon Biopsies Express Stem Cell Markers and Differentiate In Vitro. Gastroenterology
985 *138*, 1012-1021.e5. https://doi.org/10.1053/j.gastro.2009.11.052.

986 101. Young, L.M., Marzio, A., Perez-Duran, P., Reid, D.A., Meredith, D.N., Roberti, D., Star, A.,
987 Rothenberg, E., Ueberheide, B., and Pagano, M. (2015). TIMELESS Forms a Complex
988 with PARP1 Distinct from Its Complex with TIPIN and Plays a Role in the DNA Damage
989 Response. Cell Rep. *13*, 451–459. https://doi.org/10.1016/j.celrep.2015.09.017.

990 102. Sack, L.M., Davoli, T., Li, M.Z., Li, Y., Xu, Q., Naxerova, K., Wooten, E.C., Bernardi, R.J.,
991 Martin, T.D., Chen, T., et al. (2018). Profound Tissue Specificity in Proliferation Control
992 Underlies Cancer Drivers and Aneuploidy Patterns. Cell *173*, 499-514.e23.
993 https://doi.org/10.1016/j.cell.2018.02.037.

994 103. Meerbrey, K.L., Hu, G., Kessler, J.D., Roarty, K., Li, M.Z., Fang, J.E., Herschkowitz, J.I.,
995 Burrows, A.E., Ciccia, A., Sun, T., et al. (2011). The pINDUCER lentiviral toolkit for
996 inducible RNA interference in vitro and in vivo. Proc. Natl. Acad. Sci. U. S. A. *108*, 3665–
997 3670. https://doi.org/10.1073/pnas.1019736108.

998 104. Bosco, N., Goldberg, A., Zhao, X., Mays, J.C., Cheng, P., Johnson, A.F., Bianchi, J.J.,
999 Toscani, C., Di Tommaso, E., Katsnelson, L., et al. (2023). KaryoCreate: A CRISPR-based
1000 technology to study chromosome-specific aneuploidy by targeting human centromeres.
1001 Cell *186*, 1985-2001.e19. https://doi.org/10.1016/j.cell.2023.03.029.

1002 105. Fontana, P., Bonfiglio, J.J., Palazzo, L., Bartlett, E., Matic, I., and Ahel, I. (2017). Serine
1003 ADP-ribosylation reversal by the hydrolase ARH3. eLife *6*, e28533.
1004 https://doi.org/10.7554/eLife.28533.

1005 106. Dobin, A., Davis, C.A., Schlesinger, F., Drenkow, J., Zaleski, C., Jha, S., Batut, P.,
1006 Chaisson, M., and Gingeras, T.R. (2013). STAR: ultrafast universal RNA-seq aligner.
1007 Bioinforma. Oxf. Engl. *29*, 15–21. https://doi.org/10.1093/bioinformatics/bts635.

1008 107. Li, B., and Dewey, C.N. (2011). RSEM: accurate transcript quantification from RNA-Seq
1009 data with or without a reference genome. BMC Bioinformatics *12*, 323.
1010 https://doi.org/10.1186/1471-2105-12-323.

1011 108. Love, M.I., Huber, W., and Anders, S. (2014). Moderated estimation of fold change and
1012 dispersion for RNA-seq data with DESeq2. Genome Biol. *15*, 550.
1013 https://doi.org/10.1186/s13059-014-0550-8.

1014 109. Agustinus, A.S., Al-Rawi, D., Dameracharla, B., Raviram, R., Jones, B.S.C.L., Stransky,
1015 S., Scipioni, L., Luebeck, J., Di Bona, M., Norkunaite, D., et al. (2023). Epigenetic
1016 dysregulation from chromosomal transit in micronuclei. Nature *619*, 176–183.
1017 https://doi.org/10.1038/s41586-023-06084-7.

1018 110. Ghandi, M., Huang, F.W., Jané-Valbuena, J., Kryukov, G.V., Lo, C.C., McDonald, E.R.,
1019 Barretina, J., Gelfand, E.T., Bielski, C.M., Li, H., et al. (2019). Next-generation
1020 characterization of the Cancer Cell Line Encyclopedia. Nature *569*, 503–508.
1021 https://doi.org/10.1038/s41586-019-1186-3.

1022 111. Barretina, J., Caponigro, G., Stransky, N., Venkatesan, K., Margolin, A.A., Kim, S., Wilson,
1023 C.J., Lehár, J., Kryukov, G.V., Sonkin, D., et al. (2012). The Cancer Cell Line Encyclopedia
1024 enables predictive modelling of anticancer drug sensitivity. Nature *483*, 603–607.
1025 https://doi.org/10.1038/nature11003.

1026 112. Gautier, L., Cope, L., Bolstad, B.M., and Irizarry, R.A. (2004). affy—analysis of Affymetrix
1027 GeneChip data at the probe level. Bioinformatics *20*, 307–315.
1028 https://doi.org/10.1093/bioinformatics/btg405.

1029 113. Zhang, Y., Chen, F., and Creighton, C.J. (2023). Pan-cancer molecular subtypes of

1030 metastasis reveal distinct and evolving transcriptional programs. Cell Rep. Med. *4*, 100932.
1031 https://doi.org/10.1016/j.xcrm.2023.100932.

1032 114. Cox, J., and Mann, M. (2008). MaxQuant enables high peptide identification rates,
1033 individualized p.p.b.-range mass accuracies and proteome-wide protein quantification. Nat.
1034 Biotechnol. *26*, 1367–1372. https://doi.org/10.1038/nbt.1511.

1035 115. Cox, J., Neuhauser, N., Michalski, A., Scheltema, R.A., Olsen, J.V., and Mann, M. (2011).
1036 Andromeda: a peptide search engine integrated into the MaxQuant environment. J.
1037 Proteome Res. *10*, 1794–1805. https://doi.org/10.1021/pr101065j.

1038 116. Huang, T., Choi, M., Tzouros, M., Golling, S., Pandya, N.J., Banfai, B., Dunkley, T., and
1039 Vitek, O. (2020). MSstatsTMT: Statistical Detection of Differentially Abundant Proteins in
1040 Experiments with Isobaric Labeling and Multiple Mixtures. Mol. Cell. Proteomics MCP *19*,
1041 1706–1723. https://doi.org/10.1074/mcp.RA120.002105.

1042 117. Tyanova, S., Temu, T., Sinitcyn, P., Carlson, A., Hein, M.Y., Geiger, T., Mann, M., and
1043 Cox, J. (2016). The Perseus computational platform for comprehensive analysis of
1044 (prote)omics data. Nat. Methods *13*, 731–740. https://doi.org/10.1038/nmeth.3901.

1045 118. Corsello, S.M., Nagari, R.T., Spangler, R.D., Rossen, J., Kocak, M., Bryan, J.G., Humeidi,
1046 R., Peck, D., Wu, X., Tang, A.A., et al. (2020). Discovering the anti-cancer potential of non-
1047 oncology drugs by systematic viability profiling. Nat. Cancer *1*, 235–248.
1048 https://doi.org/10.1038/s43018-019-0018-6.

1049 119. Garnett, M.J., Edelman, E.J., Heidorn, S.J., Greenman, C.D., Dastur, A., Lau, K.W.,
1050 Greninger, P., Thompson, I.R., Luo, X., Soares, J., et al. (2012). Systematic identification
1051 of genomic markers of drug sensitivity in cancer cells. Nature *483*, 570–575.
1052 https://doi.org/10.1038/nature11005.

1053 120. Seashore-Ludlow, B., Rees, M.G., Cheah, J.H., Cokol, M., Price, E.V., Coletti, M.E.,
1054 Jones, V., Bodycombe, N.E., Soule, C.K., Gould, J., et al. (2015). Harnessing Connectivity
1055 in a Large-Scale Small-Molecule Sensitivity Dataset. Cancer Discov. *5*, 1210–1223.
1056 https://doi.org/10.1158/2159-8290.CD-15-0235.

1057 121. Martin, M. (2011). Cutadapt removes adapter sequences from high-throughput sequencing
1058 reads. EMBnet.journal *17*, 10–12. https://doi.org/10.14806/ej.17.1.200.

1059 122. Li, W., Xu, H., Xiao, T., Cong, L., Love, M.I., Zhang, F., Irizarry, R.A., Liu, J.S., Brown, M.,
1060 and Liu, X.S. (2014). MAGeCK enables robust identification of essential genes from
1061 genome-scale CRISPR/Cas9 knockout screens. Genome Biol. *15*, 554.
1062 https://doi.org/10.1186/s13059-014-0554-4.

1063 123. Hao, Y., Hao, S., Andersen-Nissen, E., Mauck, W.M., Zheng, S., Butler, A., Lee, M.J.,
1064 Wilk, A.J., Darby, C., Zager, M., et al. (2021). Integrated analysis of multimodal single-cell
1065 data. Cell *184*, 3573-3587.e29. https://doi.org/10.1016/j.cell.2021.04.048.

1066 124. Hafemeister, C., and Satija, R. (2019). Normalization and variance stabilization of single-
1067 cell RNA-seq data using regularized negative binomial regression. Genome Biol. *20*, 296.
1068 https://doi.org/10.1186/s13059-019-1874-1.

125. Korsunsky, I., Millard, N., Fan, J., Slowikowski, K., Zhang, F., Wei, K., Baglaenko, Y., Brenner, M., Loh, P.-R., and Raychaudhuri, S. (2019). Fast, sensitive and accurate integration of single-cell data with Harmony. Nat. Methods *16*, 1289–1296. https://doi.org/10.1038/s41592-019-0619-0.

Acknowledgments

We thank all the Davoli lab members for helpful discussions. We thank Dr. Thomas M. Norman for providing the CRISPRa Perturb-Seq data. We are grateful to Dr. Jason Sheltzer (Yale University School of Medicine) and Dr. Zuzana Storchová (TU Kaiserslautern) for the aneuploid clones generated using MMCT and their near-diploid controls. We thank Alcida Karz (NYU Grossman School of Medicine) for providing the control shRNA. We thank NYU Grossman School of Medicine's Genome Technology Center and Proteomics Laboratory for help with experiments. This research was supported by grants from the Cancer Research UK Grand Challenge, the Mark Foundation for Cancer Research (C5470/A27144), NIH R37 R37CA248631, R01 R01HG012590, R01 R01DK135089, the MRA Young Investigator Award, the Breast Cancer Alliance Young Investigator Award and a NFCR (National Foundation for Cancer Research) and by the Cancer Center Support Grant P30CA016087 at the Laura and Isaac Perlmutter Cancer Center to NYU Langone's Genome Technology Center (RRID:SCR_017929) and Proteomics Laboratory (RRID:SCR_017926). Biorender was used for some panels in Figures 1, S1, 5, 6 and S6.

List of Supplementary Materials

Supplementary Materials:

Figs. S1 to S6
Tables S1 and S7

1095 # Main Figure Legends

1096

1097 **Figure 1. Aneuploidy renders cells resistant to oxidative stress**

1098 (**A**) Acute and chronic aneuploidy models. (**B**) DNA content in diploid and aneuploid hCECs. (**C**)
1099 Viability of treated diploid and aneuploid hCECs (*TP53*WT). (**D**) Representative images of H_2O_2-
1100 treated cells (75 μM, 24h). (**E**) Viability quantification from (D). (**F**) Arm-level somatic copy number
1101 alterations in hCEC clones (*TP53*KO). (**G**) Viability of H_2O_2-treated hCEC clones (50 μM H_2O_2 for 1h
1102 + 24h release). (**H**) Viability of H_2O_2-treated HCT116 or RPE1 clones (4mM and 100 μM, respectively,
1103 24h). (**I**) Viability (top left) and representative images (right) of H_2O_2-treated KP cells (2 mM, 24h).
1104 Proliferation curves (bottom left). (**J**) Representative images and viability of H_2O_2-treated colon
1105 cancer cells (4 mM, 24 h). One-way ANOVA with Dunnett's test (C, D, HCT116 in H). Tukey's test (G,
1106 J). unpaired t-test (RPE1 in H, I). Scale bar, 50 μm.

1107

1108 **Figure 2. PARP1 is suppressed in aneuploid cells and required for ROS-induced cell death**

1109 (**A**) DNA damage in diploid and aneuploid hCECs after H_2O_2 (50 μM, 1h). Left: representative images.
1110 Right: quantification of damaged DNA. Medians with 95% CI. (**B**) Representative images of H_2O_2-
1111 treated hCECs (50 μM, 1h) with cell death inhibitors (2h pretreatment + 24h post-treatment). (**C**)
1112 Viability quantification from (B). (**D**) Relative PARP1 RNA levels (Log2) in acute aneuploidy. (**E**)
1113 PARP1 protein levels in acute aneuploidy. (**F-G**) Correlation between aneuploidy degree and PARP1
1114 RNA (F) or protein (G) levels in hCEC clones. (**H**) PARP1 protein levels in hCEC clones. (**I**) Relative
1115 PARP1 protein levels in HCT116 and RPE1 clones (data from Stingele et al., 2012). Notation: cell
1116 line-chromosome-copy number Kruskal-Wallis one-way ANOVA with Dunnett's test (A). One-way
1117 ANOVA with Dunnett's test (C, hCEC in D); Tukey's test (H). Unpaired t-test (RPE1, *TP53*KO RPE1,
1118 and HCT116 in D). One sample t-test against zero (I). Scale bar, 50 μm.

1119

1120 **Figure 3. Cell death and DNA repair mediated by PARP1 are suppressed in aneuploid cells by**
1121 **PARP1 downregulation**

1122 (**A**) PARP1 levels in near-diploid hCEC clones with PARP1 knockdown. (**B**) Viability of cells from (A)
1123 after H_2O_2. Mean ± SD of 9 fields (**C**) PARP1 levels in the acute aneuploidy (*TP53*WT hCEC) with
1124 PARP1 overexpression. Dashed lines indicate spliced lanes. (**D**) Viability of cells from (B) after H_2O_2.
1125 (**E**) PARP1 levels in aneuploid hCEC clones with PARP1 overexpression. (**F**) Viability of cells from
1126 (E) after H_2O_2. (**G**) Viability after H_2O_2 treatment with *PARP1* knockdown, PARP1 overexpression, or
1127 both. (**H**) PARP1 levels (left) and H_2O_2-induced cell viability (right) in hCECs with doxycycline-
1128 inducible PARP1 overexpression. (**I**) Viability after H_2O_2 (40 μM) with PARP1or TIMELESS
1129 overexpression or both. (**J**) Viability after H_2O_2 in hCEC clones with NMN pretreatment (180 μM,
1130 24h). (**K**) Viability after MNNG treatment (62.5 μM, 24 hours) in hCEC clones with control or PARP1
1131 overexpression. (**L**) Viability after UV (50 J/m^2 + 5-day release) in hCEC clones. Average viability

indicated below dashed line. (**M**) γH2AX before and after H_2O_2 (50 μM, 1h) in hCEC clones ± PARP1 overexpression. Left: images (scale bar, 10 μm). Right: violin plots showing median and quartiles (>460 cells/condition). R0/R6: 0 or 6h post-H_2O_2. All p-values in Table 3. γH2AX-negative threshold set at ~80% for untreated clones; percentages shown below X-axis. One-way ANOVA with Dunnett's test (B); with Tukey's test (G, I, J, K, L). Unpaired t-test (D, F, H). Kruskal-Wallis one-way ANOVA with Dunnett's test (M).

Figure 4. PARP1 suppression promotes metastasis of aneuploid cancer cells

(**A**) PARP1 levels in indicated cell lines. (**B-C**) SCNA-normalized *PARP1* RNA or protein levels in pan-cancer (B) or in colon cancer cell lines (C) with different aneuploidy degrees. (**D**) PARP1 protein in HT29 cells ± *PARP1* overexpression. (**E**) Relative viability of HT29-mCherry-EV to HT29-GFP-PARP1 when co-cultured ± H_2O_2 (2 mM, 24h). (**F**) PARP1 protein in HCT116 and DLD1 cells ± *PARP1* knockdown. (**G**) Relative viability of control vs PARP1-knockdown cells when co-cultured ± H_2O_2 (2 mM, 24h). (**H-I**) Bioluminescence images (BLI) of NSG mice with DLD1 or HCT116 ± *PARP1* knockdown. Left: representative images. Middle: total flux over time. Right: maximum values. Mean ± SD, n=5 mice/group. Crosses indicate endpoints. (**J**) BLI of immune-intact mice with aneuploid mouse KP lung cancer cells ± *PARP1* overexpression. Left: representative images. Right: maximum total flux signal. Mean + SD, n=5 mice/group. (**K**) *PARP1* RNA levels in TCGA COREAD patients without PARP1 SCNA. (**L**) Kaplan-Meier survival of TCGA COREAD patients stratified by PARP1 expression. (**M**) *PARP1* RNA levels in primary COREAD tumors and their paired metastases (n=15 patients, GSE131418). (**N**) *PARP1* RNA in unpaired primary tumors versus metastases of COREAD patients (discovery cohort: 333 primary, 184 metastases; validation cohort: 545 primary, 72 metastases, GSE131418). One-way ANOVA with Tukey's test (A, B, K). Kruskal-Wallis test, followed by one-tailed t-test comparing low vs high aneuploidy groups (C). Unpaired t-test (E, G, N). Two-tailed Mann-Whitney test (H-I). One-tailed Mann-Whitney test (J). Log-rank (Mantel-Cox) test (L). One Sample Wilcoxon signed-rank test (M).

Figure 5. Genome-wide CRISPR screen reveals lysosomal stress as a mediator of PARP1 downregulation in aneuploid cells

(**A**) FACS-based genome-wide CRISPR screen to find PARP1 regulators. (**B**) Validation of PARP1 antibody. (**C**) Enrichment and depletion of sgRNAs compared to unsorted samples. (**D**) Normalized sgPARP1 read counts in sorted vs unsorted samples. (**E**) Pathway analysis of 269 PARP1 activators. (**F**) PCA of lysosomal (left) and proteasomal (right) gene expression in near-diploid (blue) and aneuploid (red) hCEC clones. Group separation assessed by 10,000 permutations using Euclidean distances in PC1-PC2 space. (**G**) Heatmap of log2FC z-scores for KEGG lysosomal genes in aneuploid cells and Bafilomycin A1 (Baf A1)-treated cells. (**H**) Spearman correlation of lysosomal gene expression changes in aneuploid cells and Baf A1-treated RPE1 cells. (**I**) *PARP1* mRNA levels (Log2) in Baf A1-treated cells. (**J**) Viability of hCECs pre-treated with Baf A1 (5 nM, 24h) followed by

1170 H_2O_2 (200 μM, 24 h). (**K**) Viability after H_2O_2 in hCECs ± Baf A1 pre-treatment or PARP1
1171 overexpression. One-way ANOVA with Dunnetts' test (D); with Tukey's test (K). Unpaired t-test (I, J).
1172
1173 **Figure 6. Aneuploidy-activated CEBPB transcription factor suppresses PARP1**
1174 (**A**) Top: Strategy to identify transcription factors (TFs) regulating *PARP1* expression in aneuploid
1175 cells. Bottom: Heatmap showing PARP1-promoting and PARP1-suppressing TFs and their
1176 expression changes across lysosome-deficient and aneuploid models. $p<0.05$. (**B**) CEBPB ChIP-
1177 Seq data (ENCODE) near the PARP1 transcription start site. (**C**) CEBPB RNA and protein levels in
1178 acute aneuploidy models. (**D**) Nuclear CEBPB in hCECs with acute and chronic aneuploidy. Left:
1179 representative images (scale bar, 10 μm). Right: quantification of nuclear CEBPB. n>50
1180 cells/condition. (**E**) *CEBPB* RNA (left) and protein (right) correlation with aneuploidy score in
1181 aneuploid clones. (**F**) *CEBPB* RNA in Baf A1-treated cells (published dataset). (**G**) Normalized
1182 sgCEBPB read counts in sorted samples versus unsorted samples. (**H**) PARP1 protein after *CEBPB*
1183 overexpression. (**I**) CRISPR activation (CRISPRa) Perturb-Seq analysis of PARP1 regulation by
1184 CEBPB. (Left) CEBPB and PARP1 levels in cells with CEBPB CRISPRa (sgCEBPB-1) versus control
1185 (sgNC). (Right) PARP1 expression heatmap following CEBPB activation. (**J**) scRNA-seq analysis of
1186 malignant colorectal cancer cells. UMAP plots displaying cell density for cells with top 30% of
1187 CEBPB expression (upper left), top 30% of PARP1 expression (upper right), aneuploidy score >5
1188 (lower left), and top 30% of KEGG lysosome signature score (lower right). Cell density is weighted
1189 by the respective scores. Populations with high CEBPB expression, high aneuploidy, and high
1190 lysosomal activity (red arrows) overlap but are distinct from populations with high PARP1
1191 expression (blue arrows). (**K**) *CEBPB* and *PARP1* RNA level correlation in pan-cancer cell lines. (**L**)
1192 Viability after H_2O_2 in *CEBPB*-OE versus EV cells (40 μM for *TP53*-KO hCEC, 2 mM for DLD1, 24h).
1193 One-way ANOVA with Dunnett's test (hCEC in C, G); with Tukey's test (hCEC clones in D). Unpaired
1194 t-test (RPE1, RPE1-*TP53*KO and HCT116 in C, acute aneuploidy in D, F, H, I, L).

Figure 1

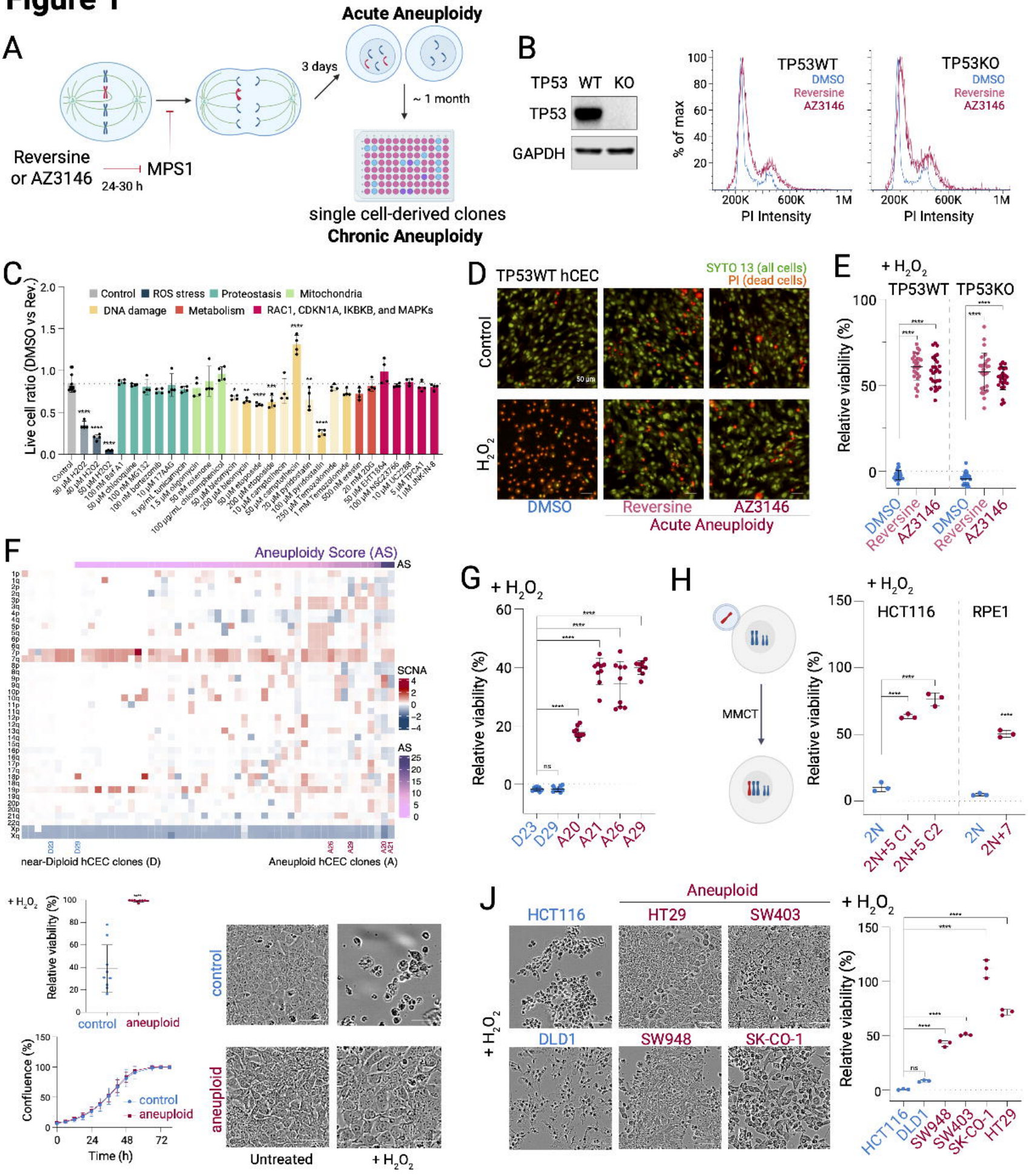
A
Acute Aneuploidy
3 days
~ 1 month
Reversine or AZ3146
MPS1
24-30 h
single cell-derived clones
Chronic Aneuploidy
B
TP53 WT KO
TP53
GAPDH
TP53WT
TP53KO
DMSO
Reversine
AZ3146
% of max
PI Intensity
C
Control
ROS stress
Proteostasis
Mitochondria
DNA damage
Metabolism
RAC1, CDKN1A, IKBKB, and MAPKs
Live cell ratio (DMSO vs Rev.)
D
TP53WT hCEC
SYTO 13 (all cells)
PI (dead cells)
Control
H2O2
DMSO
Reversine
AZ3146
Acute Aneuploidy
E
+ H2O2
TP53WT
TP53KO
Relative viability (%)
F
Aneuploidy Score (AS)
SCNA
AS
near-Diploid hCEC clones (D)
Aneuploid hCEC clones (A)
G
+ H2O2
Relative viability (%)
D23
D29
A20
A21
A26
A29
H
MMCT
+ H2O2
HCT116
RPE1
2N
2N+5 C1
2N+5 C2
2N+7
I
+ H2O2
Relative viability (%)
control
aneuploid
Confluence (%)
Time (h)
Untreated
+ H2O2
J
Aneuploid
HCT116
HT29
SW403
DLD1
SW948
SK-CO-1
+ H2O2
Relative viability (%)

Figure 2

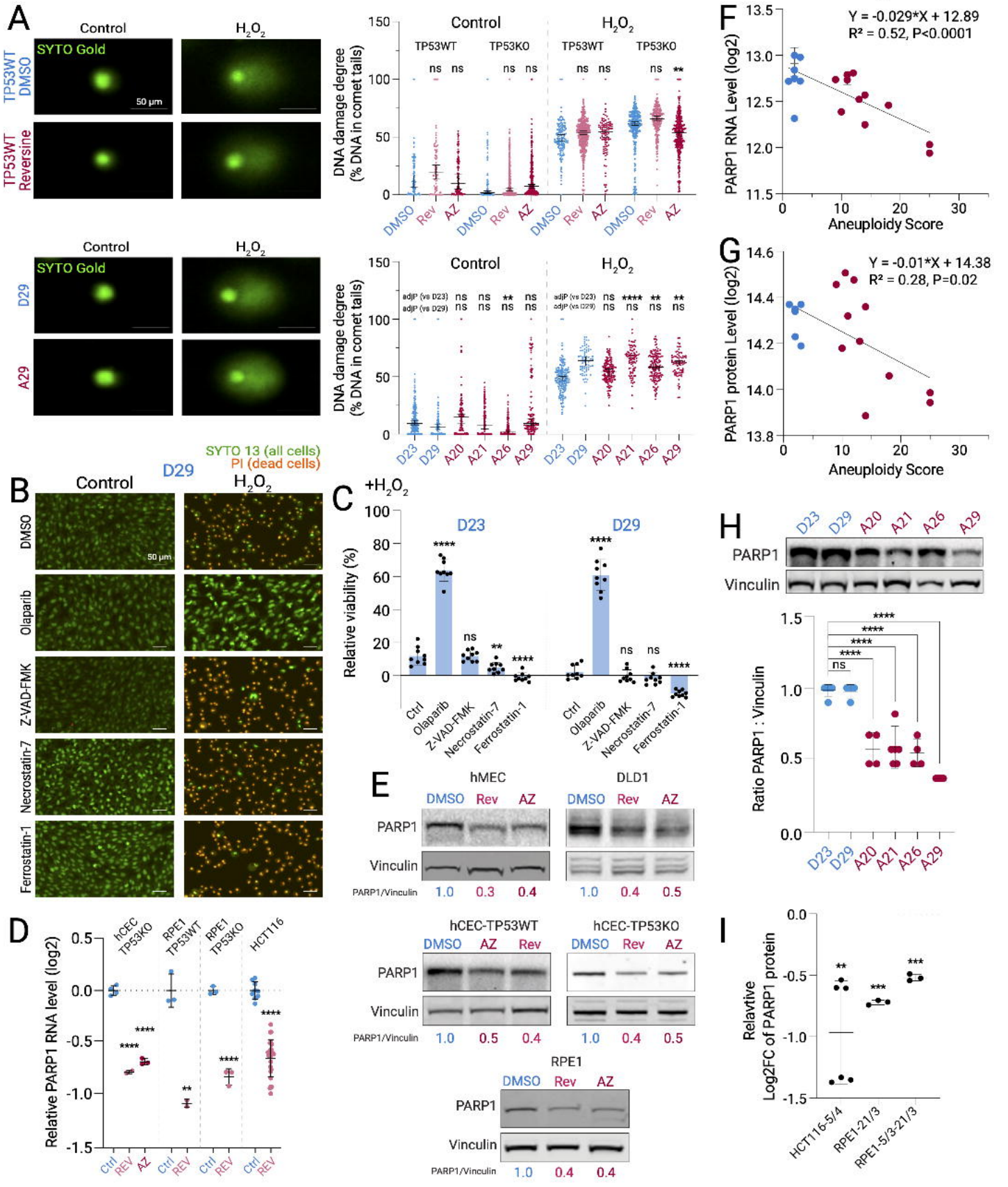
A
Control
H2O2
SYTO Gold
TP53WT DMSO
TP53WT Reversine
50 µm
DNA damage degree (% DNA in comet tails)
TP53WT
TP53KO
DMSO
Rev
AZ
D29
A29
D23
A20
A21
A26
B
SYTO 13 (all cells)
PI (dead cells)
Olaparib
Z-VAD-FMK
Necrostatin-7
Ferrostatin-1
C
+H2O2
Relative viability (%)
Ctrl
D
Relative PARP1 RNA level (log2)
hCEC TP53KO
RPE1 TP53WT
RPE1 TP53KO
HCT116
REV
E
hMEC
DLD1
hCEC-TP53WT
hCEC-TP53KO
RPE1
PARP1
Vinculin
PARP1/Vinculin
F
Y = -0.029*X + 12.89
R² = 0.52, P<0.0001
PARP1 RNA Level (log2)
Aneuploidy Score
G
Y = -0.01*X + 14.38
R² = 0.28, P=0.02
PARP1 protein Level (log2)
H
Ratio PARP1 : Vinculin
I
Relavtive Log2FC of PARP1 protein
HCT116-5/4
RPE1-21/3
RPE1-5/3-21/3

Figure 3

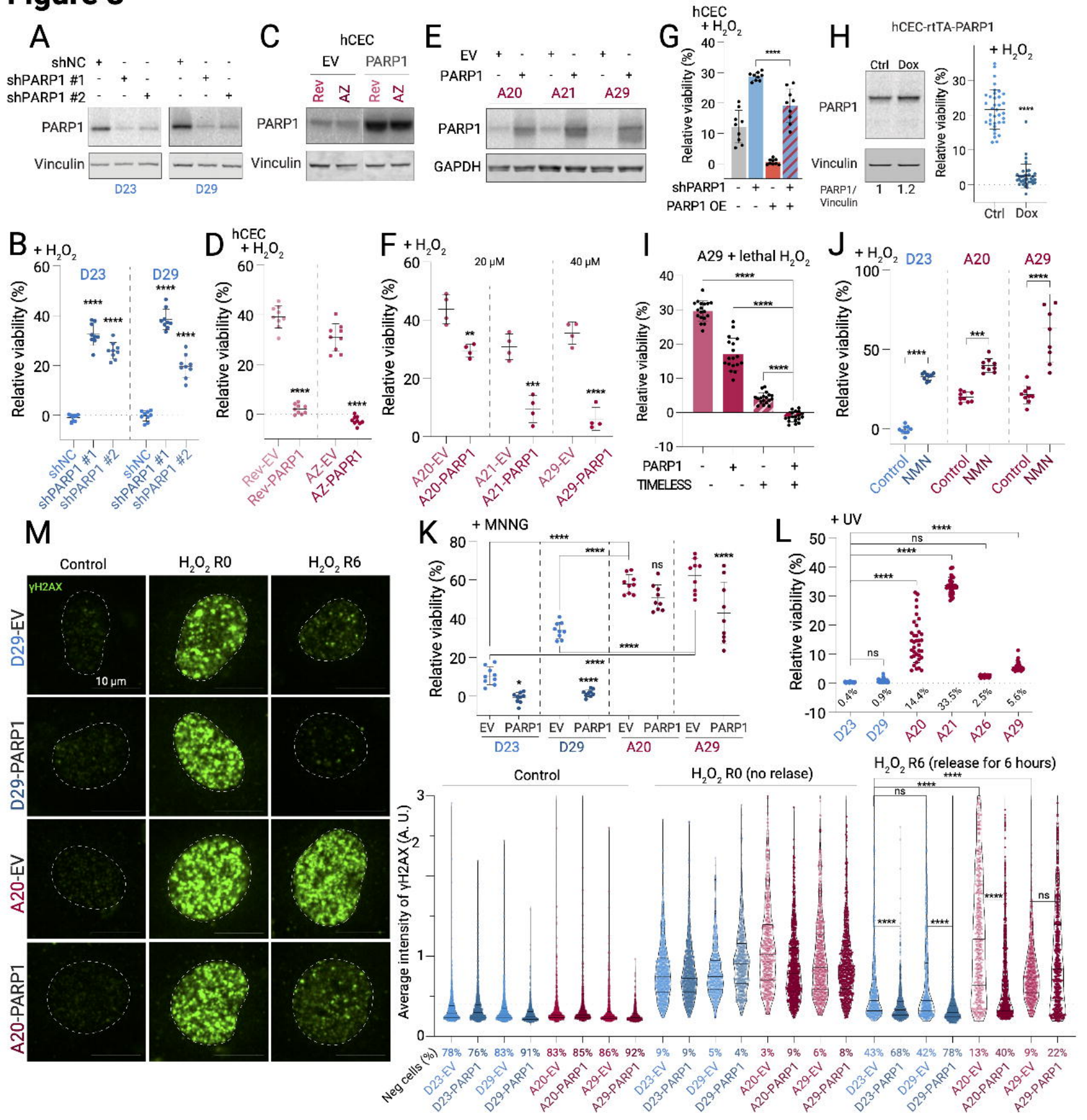
A
shNC
shPARP1 #1
shPARP1 #2
PARP1
Vinculin
D23
D29
C
hCEC
EV
PARP1
Rev
AZ
PARP1
Vinculin
E
EV
PARP1
A20
A21
A29
PARP1
GAPDH
G
hCEC
+ H2O2
Relative viability (%)
shPARP1
PARP1 OE
H
hCEC-rtTA-PARP1
Ctrl
Dox
PARP1
Vinculin
PARP1/ Vinculin
1
1.2
+ H2O2
Relative viability (%)
Ctrl
Dox
B
+ H2O2
D23
D29
Relative viability (%)
shNC
shPARP1 #1
shPARP1 #2
D
hCEC
+ H2O2
Relative viability (%)
Rev-EV
Rev-PARP1
AZ-EV
AZ-PAPR1
F
+ H2O2
20 μM
40 μM
Relative viability (%)
A20-EV
A20-PARP1
A21-EV
A21-PARP1
A29-EV
A29-PARP1
I
A29 + lethal H2O2
Relative viability (%)
PARP1
TIMELESS
J
+ H2O2
D23
A20
A29
Relative viability (%)
Control
NMN
M
Control
H2O2 R0
H2O2 R6
γH2AX
10 μm
D29-EV
D29-PARP1
A20-EV
A20-PARP1
K
+ MNNG
Relative viability (%)
EV
PARP1
D23
D29
A20
A29
L
+ UV
Relative viability (%)
0.4%
0.9%
14.4%
33.5%
2.5%
5.6%
D23
D29
A20
A21
A26
A29
Control
H2O2 R0 (no relase)
H2O2 R6 (release for 6 hours)
Average intensity of γH2AX (A. U.)
Neg cells (%)
78% 76% 83% 91% 83% 85% 86% 92% 9% 9% 5% 4% 3% 9% 6% 8% 43% 68% 42% 78% 13% 40% 9% 22%
D23-EV
D23-PARP1
D29-EV
D29-PARP1
A20-EV
A20-PARP1
A29-EV
A29-PARP1

Figure 4

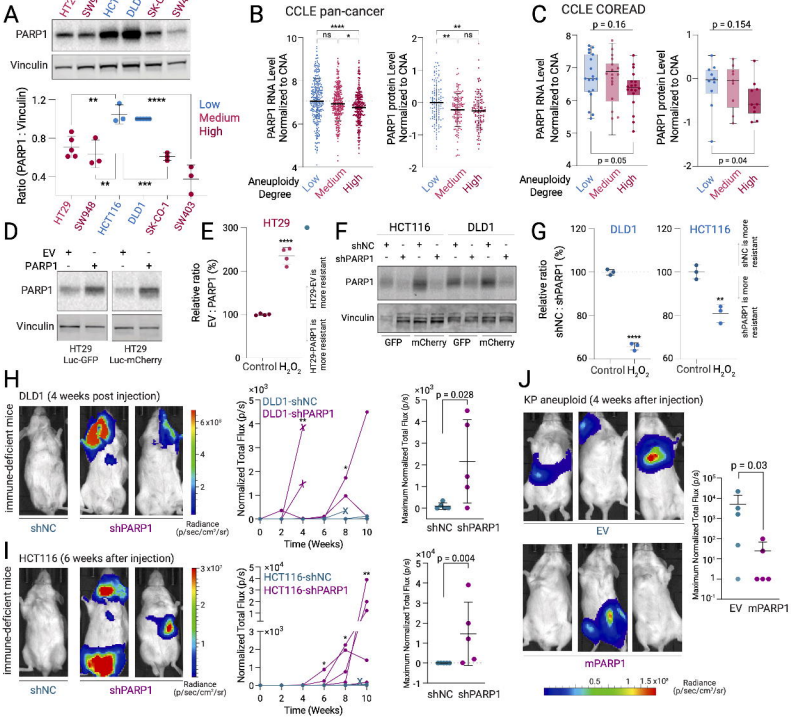
A
HT29
SW948
HCT116
DLD1
SK-CO-1
SW403
PARP1
Vinculin
Ratio (PARP1 : Vinculin)
Low
Medium
High
B
CCLE pan-cancer
PARP1 RNA Level Normalized to CNA
PARP1 protein Level Normalized to CNA
Aneuploidy Degree
C
CCLE COREAD
p = 0.16
p = 0.05
p = 0.154
p = 0.04
D
EV
PARP1
HT29 Luc-GFP
HT29 Luc-mCherry
E
HT29
Relative ratio EV : PARP1 (%)
HT29-EV is more resistant
HT29-PARP1 is more resistant
Control
H2O2
F
HCT116
DLD1
shNC
shPARP1
GFP
mCherry
G
DLD1
HCT116
Relative ratio shNC : shPARP1 (%)
shNC is more resistant
shPARP1 is more resistant
H
DLD1 (4 weeks post injection)
immune-deficient mice
shNC
shPARP1
Radiance (p/sec/cm²/sr)
DLD1-shNC
DLD1-shPARP1
Normalized Total Flux (p/s)
Time (Weeks)
p = 0.028
Maximum Normalized Total Flux (p/s)
I
HCT116 (6 weeks after injection)
HCT116-shNC
HCT116-shPARP1
p = 0.004
J
KP aneuploid (4 weeks after injection)
EV
mPARP1
p = 0.03
K
TCGA COREAD
PARP1 RNA Level (FPKM)
L
TCGA COREAD
Probability of Survival
p = 0.007
PARP1-Low (n=124)
PARP1-High (n=473)
years
M
Kamal et al. 2019 paired
PARP1 RNA
13.3%
73.3%
Primary
Metastasis
N
Kamal et al. 2019 unpaired discovery
Kamal et al. 2019 unpaired validation

Figure 5

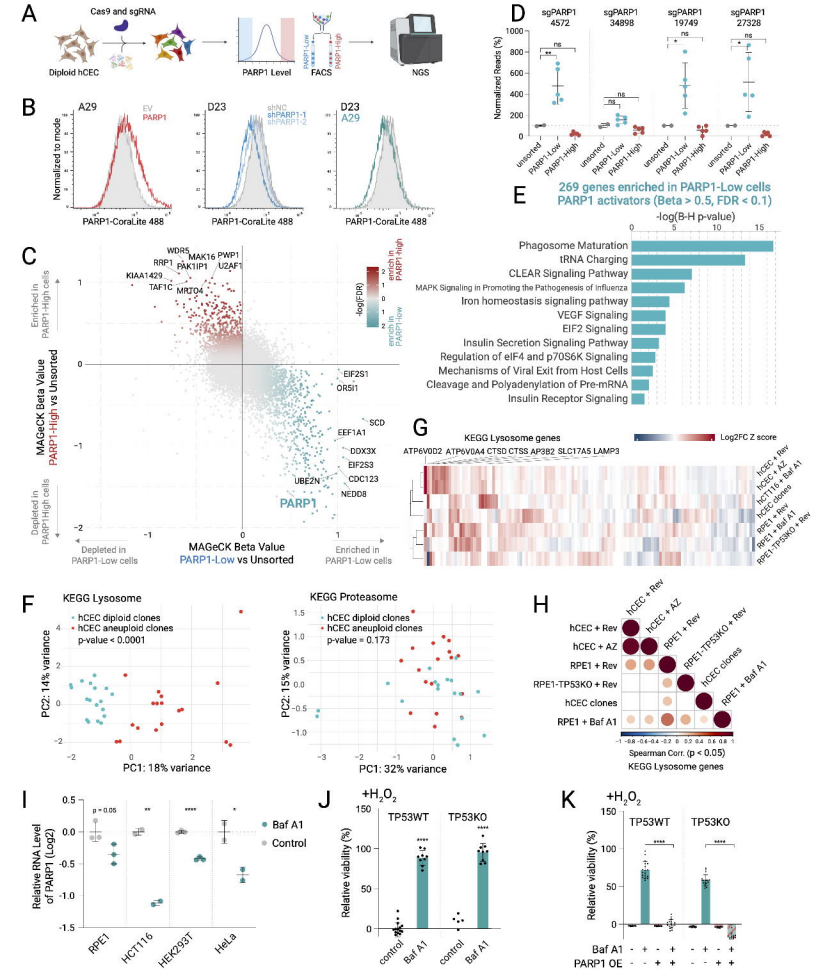
A
Cas9 and sgRNA
Diploid hCEC
PARP1 Level
FACS
PARP1-Low
PARP1-High
NGS
B
A29
EV
PARP1
D23
shNC
shPARP1-1
shPARP1-2
D23
A29
Normalized to mode
PARP1-CoraLite 488
C
MAGeCK Beta Value
PARP1-High vs Unsorted
Enriched in PARP1-High cells
Depleted in PARP1High cells
Depleted in PARP1-Low cells
Enriched in PARP1-Low cells
MAGeCK Beta Value
PARP1-Low vs Unsorted
-log(FDR)
enriched in PARP1-High
enriched in PARP1-Low
WDR5
MAK16
PWP1
RRP1
PAK1IP1
U2AF1
KIAA1429
TAF1C
MRT04
EIF2S1
ORS1
SCD
EEF1A1
DDX3X
EIF2S3
CDC123
UBE2N
NEDD8
PARP1
D
sgPARP1 4572
sgPARP1 34898
sgPARP1 19749
sgPARP1 27328
Normalized Reads (%)
unsorted
PARP1-Low
PARP1-High
E
269 genes enriched in PARP1-Low cells
PARP1 activators (Beta > 0.5, FDR < 0.1)
-log(B-H p-value)
Phagosome Maturation
tRNA Charging
CLEAR Signaling Pathway
MAPK Signaling in Promoting the Pathogenesis of Influenza
Iron homeostasis signaling pathway
VEGF Signaling
EIF2 Signaling
Insulin Secretion Signaling Pathway
Regulation of eIF4 and p70S6K Signaling
Mechanisms of Viral Exit from Host Cells
Cleavage and Polyadenylation of Pre-mRNA
Insulin Receptor Signaling
F
KEGG Lysosome
hCEC diploid clones
hCEC aneuploid clones
p-value < 0.0001
PC2: 14% variance
PC1: 18% variance
KEGG Proteasome
hCEC diploid clones
hCEC aneuploid clones
p-value = 0.173
PC2: 15% variance
PC1: 32% variance
G
KEGG Lysosome genes
Log2FC Z score
ATP6V0D2 ATP6V0A4 CTSD CTSS AP3B2 SLC17A5 LAMP3
hCEC + Rev
hCEC + AZ
hCEC + Baf A1
hCEC clones
RPE1 + Rev
RPE1 + Baf A1
RPE1-TP53KO + Rev
H
hCEC + Rev
hCEC + AZ
RPE1 + Rev
RPE1-TP53KO + Rev
hCEC clones
RPE1 + Baf A1
Spearman Corr. (p < 0.05)
KEGG Lysosome genes
I
Relative RNA Level of PARP1 (Log2)
p = 0.05
Baf A1
Control
RPE1
HCT116
HEK293T
HeLa
J
+H2O2
TP53WT
TP53KO
Relative viability (%)
control
Baf A1
K
+H2O2
TP53WT
TP53KO
Relative viability (%)
Baf A1
PARP1 OE

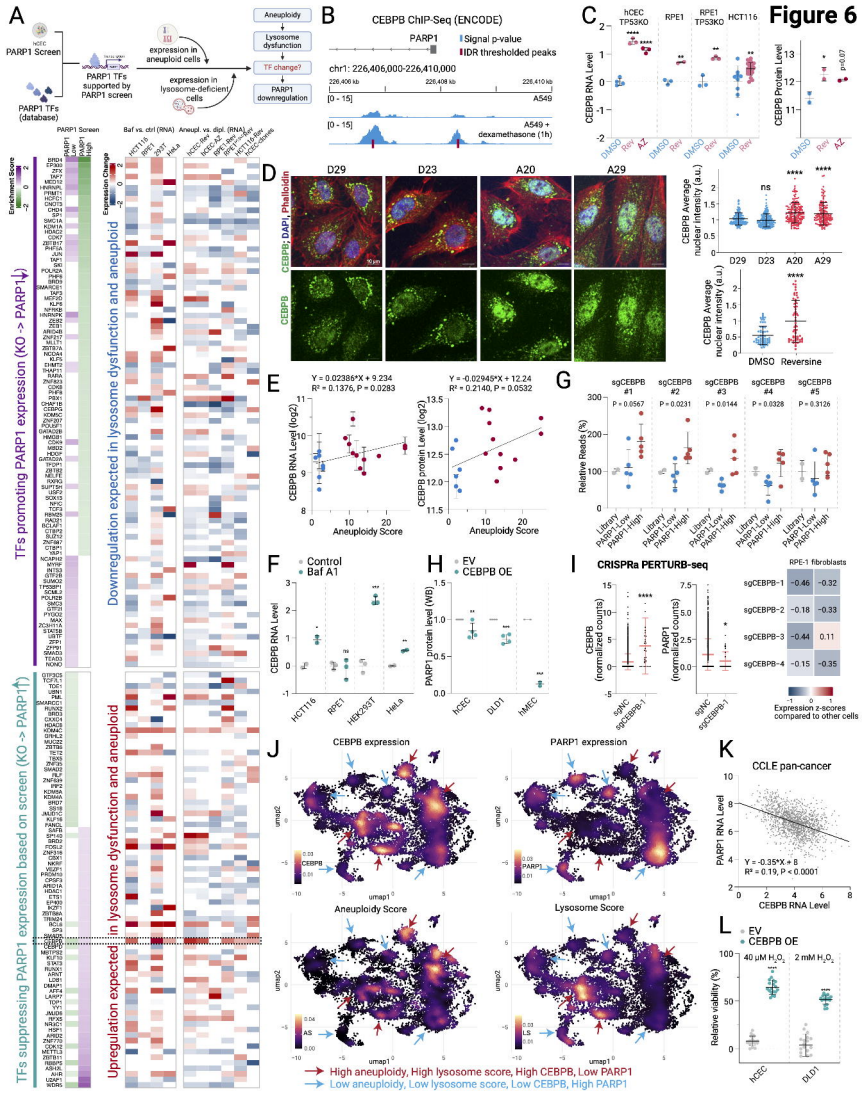
Figure 6
A
PARP1 Screen
PARP1 TFs (database)
PARP1 TFs supported by PARP1 screen
expression in aneuploid cells
expression in lysosome-deficient cells
Aneuploidy
Lysosome dysfunction
TF change?
PARP1 downregulation
B
CEBPB ChIP-Seq (ENCODE)
PARP1
chr1: 226,406,000-226,410,000
Signal p-value
IDR thresholded peaks
A549 + dexamethasone (1h)
C
hCEC TP53KO
RPE1
RPE1 TP53KO
HCT116
CEBPB RNA Level
CEBPB Protein Level
DMSO
Rex
AZ
D
D29
D23
A20
A29
CEBPB; DAPI, Phalloidin
CEBPB
CEBPB Average nuclear intensity (a.u.)
Reversine
E
Y = 0.02386*X + 9.234
R² = 0.1376, P = 0.0283
Y = -0.02945*X + 12.24
R² = 0.2140, P = 0.0532
CEBPB RNA Level (log2)
CEBPB protein Level (log2)
Aneuploidy Score
F
Control
Baf A1
CEBPB RNA Level
HCT116
RPE1
HEK293T
HeLa
G
sgCEBPB #1
sgCEBPB #2
sgCEBPB #3
sgCEBPB #4
sgCEBPB #5
Relative Reads (%)
Library
PARP1 Low
PARP1 High
H
EV
CEBPB OE
PARP1 protein level (WB)
hCEC
DLD1
hMEC
I
CRISPRa PERTURB-seq
CEBPB (normalized counts)
PARP1 (normalized counts)
sgNC
sgCEBPB-1
RPE-1 fibroblasts
sgCEBPB-1 -0.46 -0.32
sgCEBPB-2 -0.18 -0.33
sgCEBPB-3 -0.44 0.11
sgCEBPB-4 -0.15 -0.35
Expression z-scores compared to other cells
J
CEBPB expression
PARP1 expression
Aneuploidy Score
Lysosome Score
umap1
umap2
High aneuploidy, High lysosome score, High CEBPB, Low PARP1
Low aneuploidy, Low lysosome score, Low CEBPB, High PARP1
K
CCLE pan-cancer
PARP1 RNA Level
CEBPB RNA Level
Y = -0.35*X + 8
R² = 0.19, P < 0.0001
L
EV
CEBPB OE
40 μM H2O2
2 mM H2O2
Relative viability (%)
hCEC
DLD1
PARP1 Screen
Baf vs. ctrl (RNA)
Aneupl. vs. dipl. (RNA)
Enrichment Score
Expression Change
TFs promoting PARP1 expression (KO -> PARP1↓)
Downregulation expected in lysosome dysfunction and aneuploid
TFs suppressing PARP1 expression based on screen (KO -> PARP1↑)
Upregulation expected in lysosome dysfunction and aneuploid

PARP1 is suppressed in aneuploid cells via lysosomal stress and CEBPB activation

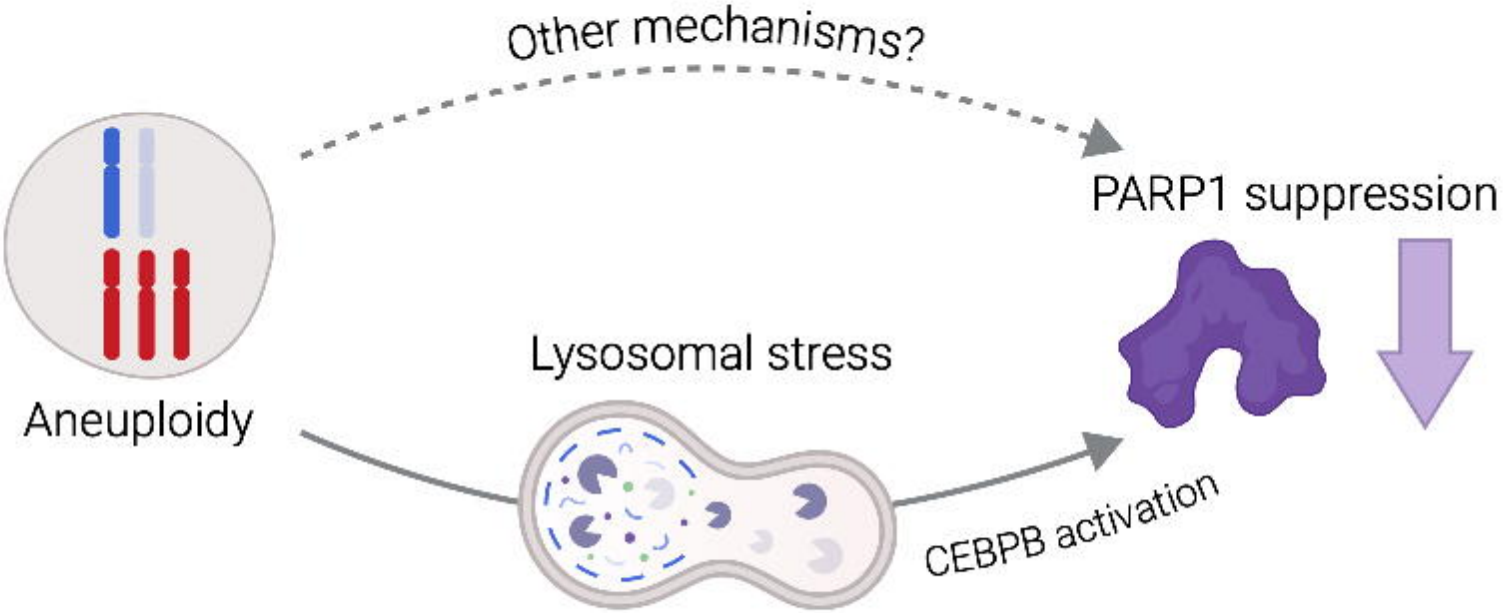

PARP1 suppression inhibits cell death and DNA repair, and promotes metastasis

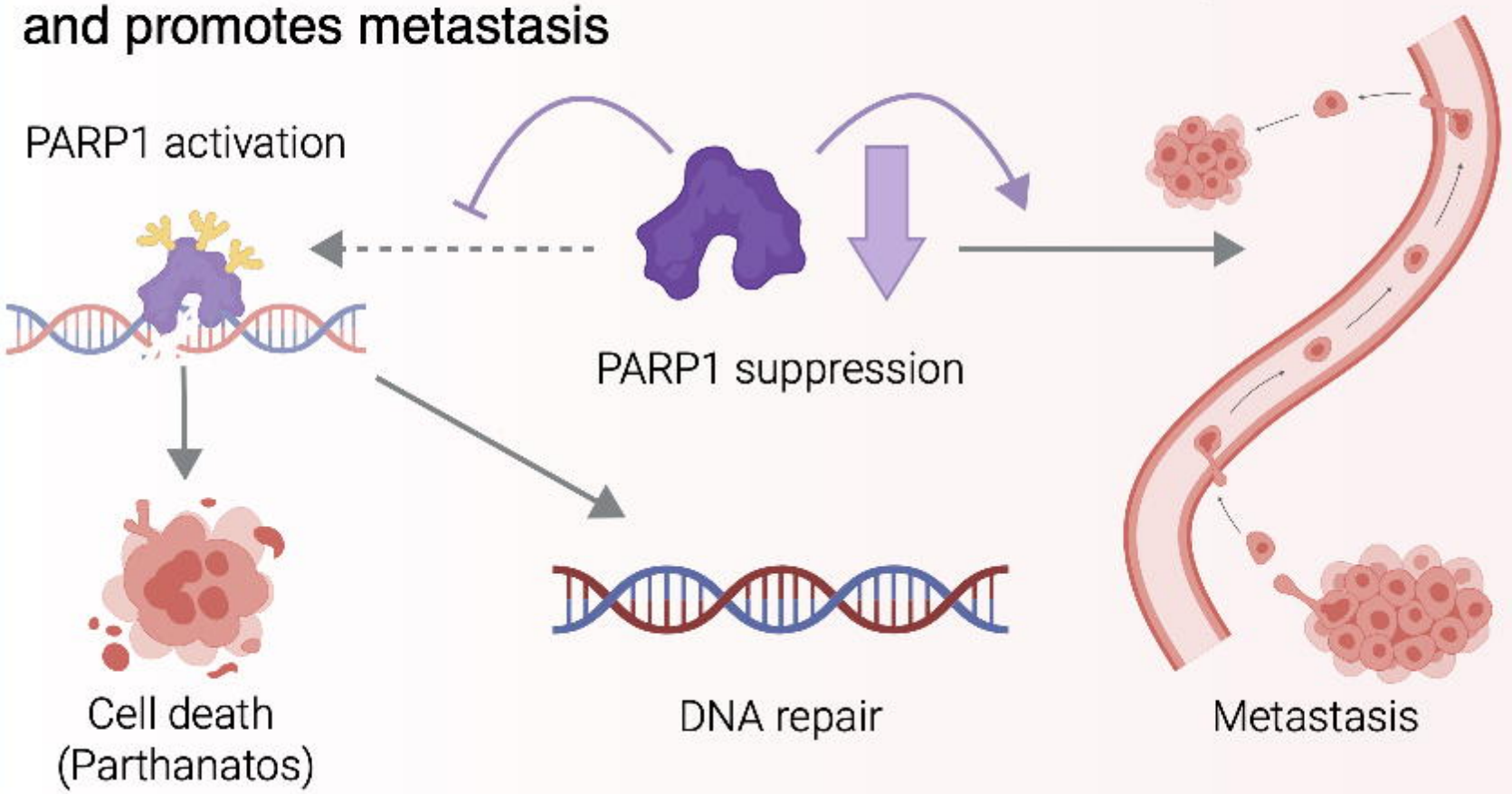

Figure S1

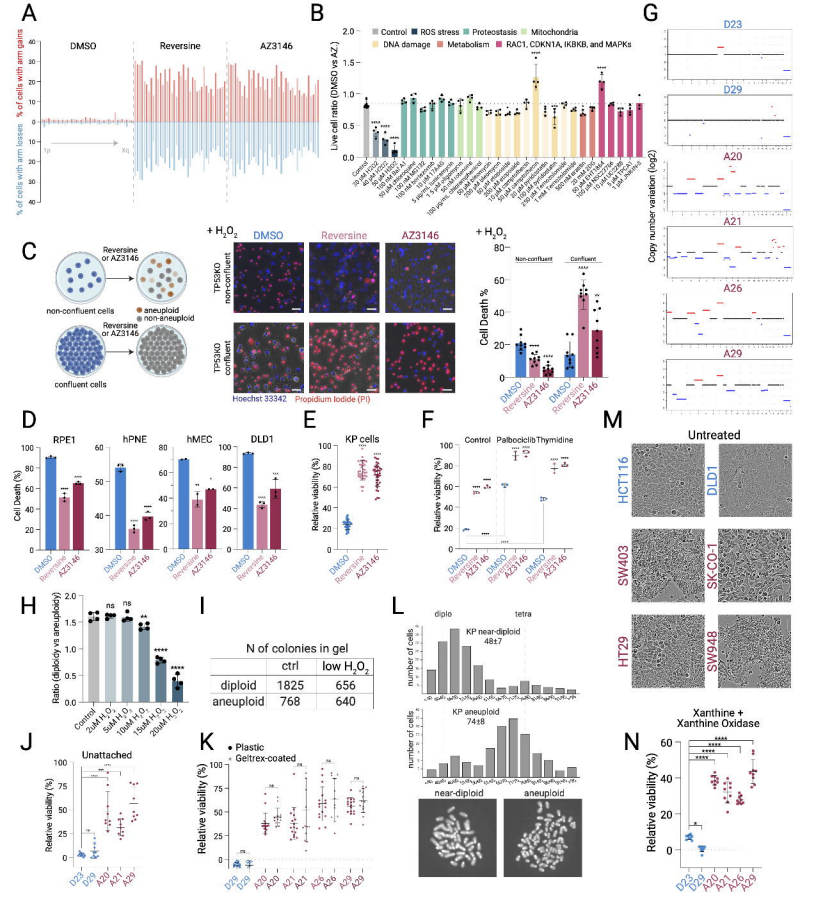
A
DMSO
Reversine
AZ3146
% of cells with arm gains
% of cells with arm losses
1p
Xq
B
Control
ROS stress
Proteostasis
Mitochondria
DNA damage
Metabolism
RAC1, CDKN1A, IKBKB, and MAPKs
Live cell ratio (DMSO vs AZ)
C
Reversine or AZ3146
non-confluent cells
aneuploid
non-aneuploid
confluent cells
+ H2O2
DMSO
Reversine
AZ3146
TP53KO non-confluent
TP53KO confluent
Hoechst 33342
Propidium Iodide (PI)
Non-confluent
Confluent
Cell Death %
D
RPE1
hPNE
hMEC
DLD1
Cell Death (%)
E
KP cells
Relative viability (%)
F
Control
Palbociclib
Thymidine
Relative viability (%)
G
D23
D29
A20
A21
A26
A29
Copy number variation (log2)
H
Ratio (diploid vs aneuploid)
Control
2uM H2O2
5uM H2O2
10uM H2O2
15uM H2O2
20uM H2O2
I
N of colonies in gel
ctrl
low H2O2
diploid 1825 656
aneuploid 768 640
J
Unattached
Relative viability (%)
K
Plastic
Geltrex-coated
Relative viability (%)
L
diploid
tetra
KP near-diploid
48±7
KP aneuploid
74±8
number of cells
near-diploid
aneuploid
M
Untreated
HCT116
DLD1
SW403
SK-CO-1
HT29
SW948
N
Xanthine + Xanthine Oxidase
Relative viability (%)

Figure S2

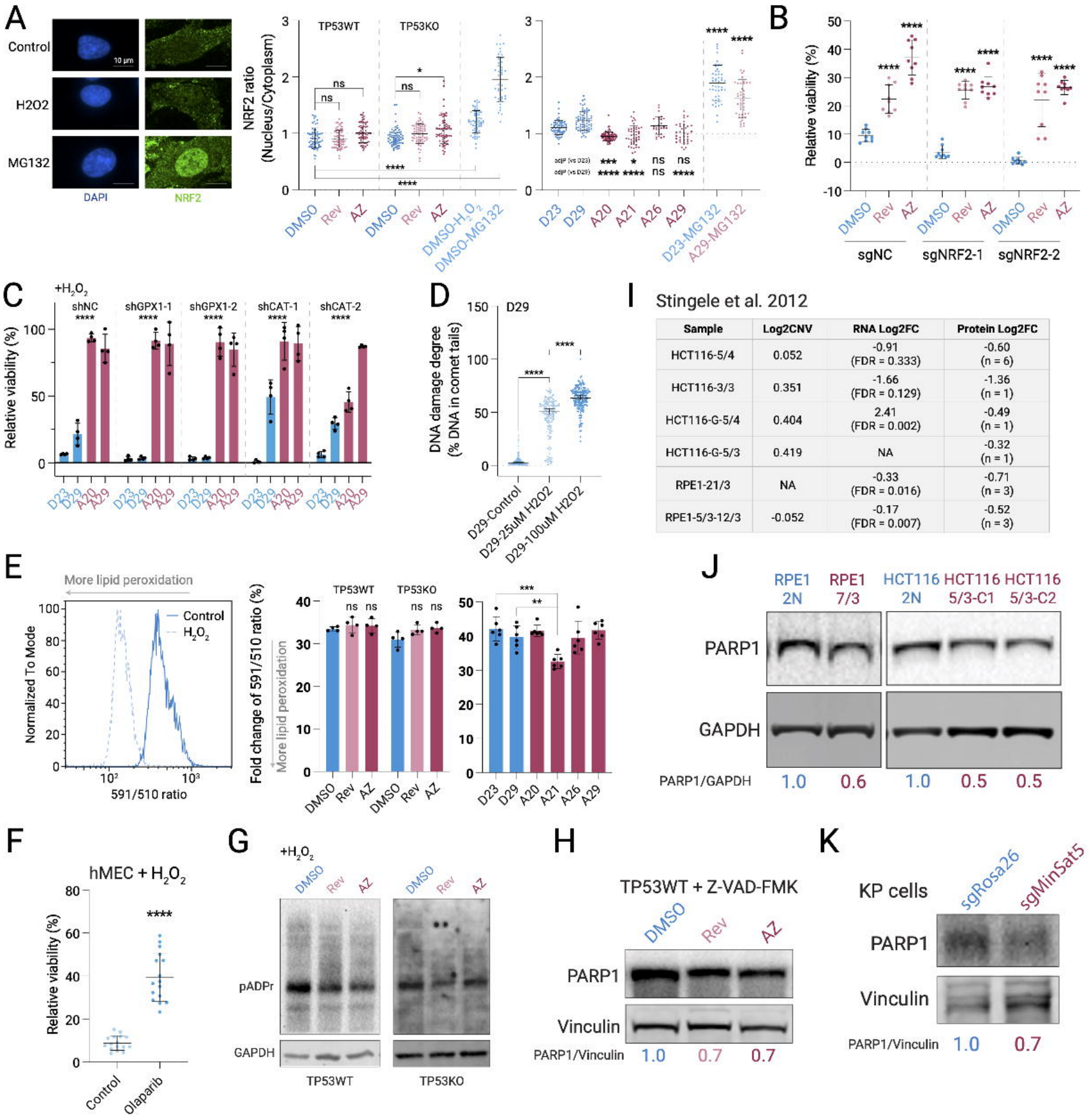
A
Control
H2O2
MG132
DAPI
NRF2
10 µm
NRF2 ratio (Nucleus/Cytoplasm)
TP53WT
TP53KO
DMSO
Rev
AZ
DMSO-H2O2
DMSO-MG132
D23
D29
A20
A21
A26
A29
D23-MG132
A29-MG132
B
Relative viability (%)
sgNC
sgNRF2-1
sgNRF2-2
C
+H2O2
shNC
shGPX1-1
shGPX1-2
shCAT-1
shCAT-2
Relative viability (%)
D
D29
DNA damage degree (% DNA in comet tails)
D29-Control
D29-25uM H2O2
D29-100uM H2O2
I
Stingele et al. 2012
Sample | Log2CNV | RNA Log2FC | Protein Log2FC
HCT116-5/4 | 0.052 | -0.91 (FDR = 0.333) | -0.60 (n = 6)
HCT116-3/3 | 0.351 | -1.66 (FDR = 0.129) | -1.36 (n = 1)
HCT116-G-5/4 | 0.404 | 2.41 (FDR = 0.002) | -0.49 (n = 1)
HCT116-G-5/3 | 0.419 | NA | -0.32 (n = 1)
RPE1-21/3 | NA | -0.33 (FDR = 0.016) | -0.71 (n = 3)
RPE1-5/3-12/3 | -0.052 | -0.17 (FDR = 0.007) | -0.52 (n = 3)
E
More lipid peroxidation
Control
H2O2
Normalized To Mode
591/510 ratio
Fold change of 591/510 ratio (%)
More lipid peroxidation
TP53WT
TP53KO
J
RPE1 2N
RPE1 7/3
HCT116 2N
HCT116 5/3-C1
HCT116 5/3-C2
PARP1
GAPDH
PARP1/GAPDH
1.0
0.6
1.0
0.5
0.5
F
hMEC + H2O2
Relative viability (%)
Control
Olaparib
G
+H2O2
DMSO
Rev
AZ
pADPr
GAPDH
TP53WT
TP53KO
H
TP53WT + Z-VAD-FMK
DMSO
Rev
AZ
PARP1
Vinculin
PARP1/Vinculin
1.0
0.7
0.7
K
KP cells
sgRosa26
sgMinSat5
PARP1
Vinculin
PARP1/Vinculin
1.0
0.7

Figure S3

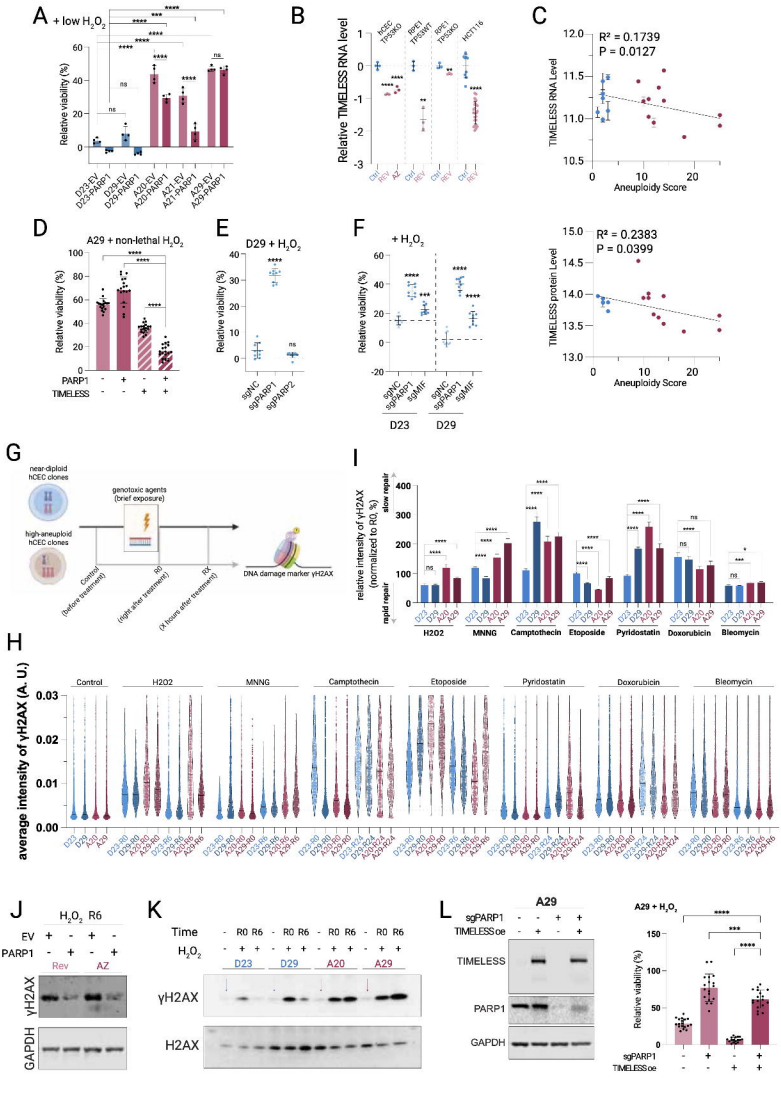
A
+ low H2O2
Relative viability (%)
D23 EV
D23 PARP1
D29 EV
D29 PARP1
A20 EV
A20 PARP1
A21 EV
A21 PARP1
A29 EV
A29 PARP1
B
Relative TIMELESS RNA level
hCEC
TP53KO
RPE1
TP53WT
RPE1
TP53KO
HCT116
Ctrl
REV
AZ
C
R² = 0.1739
P = 0.0127
TIMELESS RNA Level
Aneuploidy Score
D
A29 + non-lethal H2O2
Relative viability (%)
PARP1
TIMELESS
E
D29 + H2O2
Relative viability (%)
sgNC
sgPARP1
sgPARP2
F
+ H2O2
Relative viability (%)
sgNC
sgPARP1
sgMIF
D23
D29
R² = 0.2383
P = 0.0399
TIMELESS protein Level
Aneuploidy Score
G
near-diploid hCEC clones
high-aneuploid hCEC clones
genotoxic agents (brief exposure)
Control (before treatment)
R0 (right after treatment)
R2 (X hours after treatment)
DNA damage marker γH2AX
I
relative intensity of γH2AX (normalized to R0, %)
slow repair
rapid repair
H2O2
MNNG
Camptothecin
Etoposide
Pyridostatin
Doxorubicin
Bleomycin
H
average intensity of γH2AX (A. U.)
Control
H2O2
MNNG
Camptothecin
Etoposide
Pyridostatin
Doxorubicin
Bleomycin
J
H2O2 R6
EV
PARP1
Rev
AZ
γH2AX
GAPDH
K
Time
H2O2
D23
D29
A20
A29
γH2AX
H2AX
L
A29
sgPARP1
TIMELESSoe
TIMELESS
PARP1
GAPDH
A29 + H2O2
Relative viability (%)
sgPARP1
TIMELESSoe

Figure S4

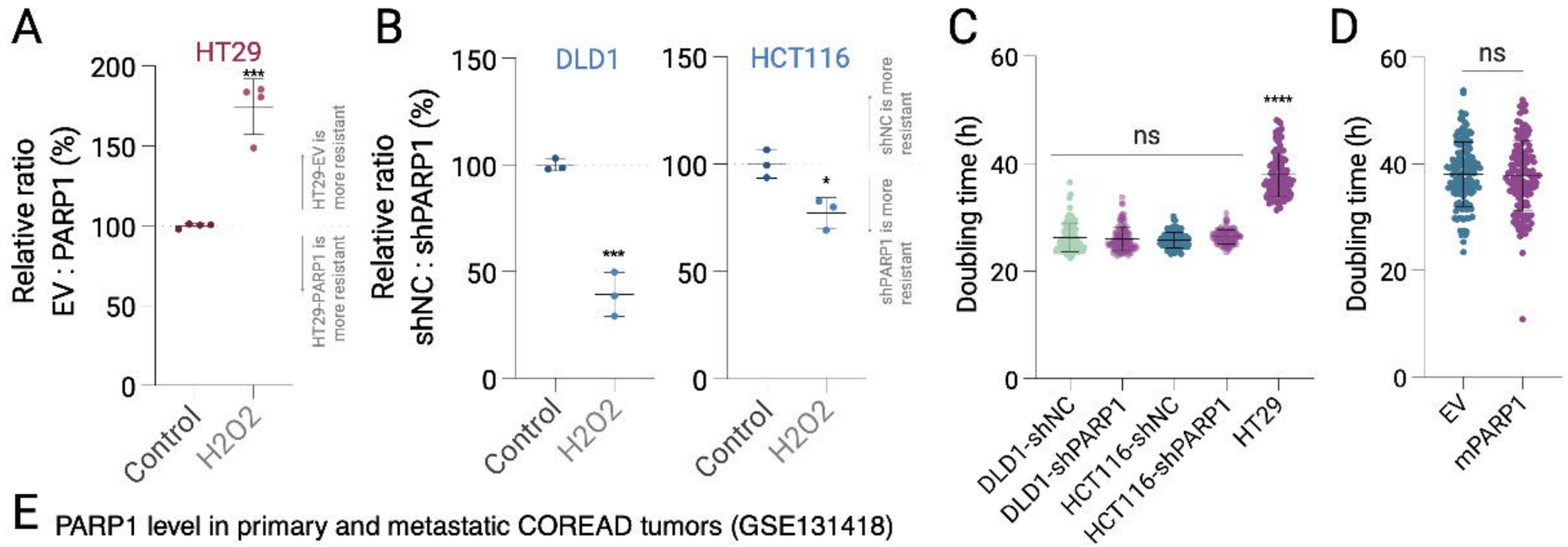

E PARP1 level in primary and metastatic COREAD tumors (GSE131418)

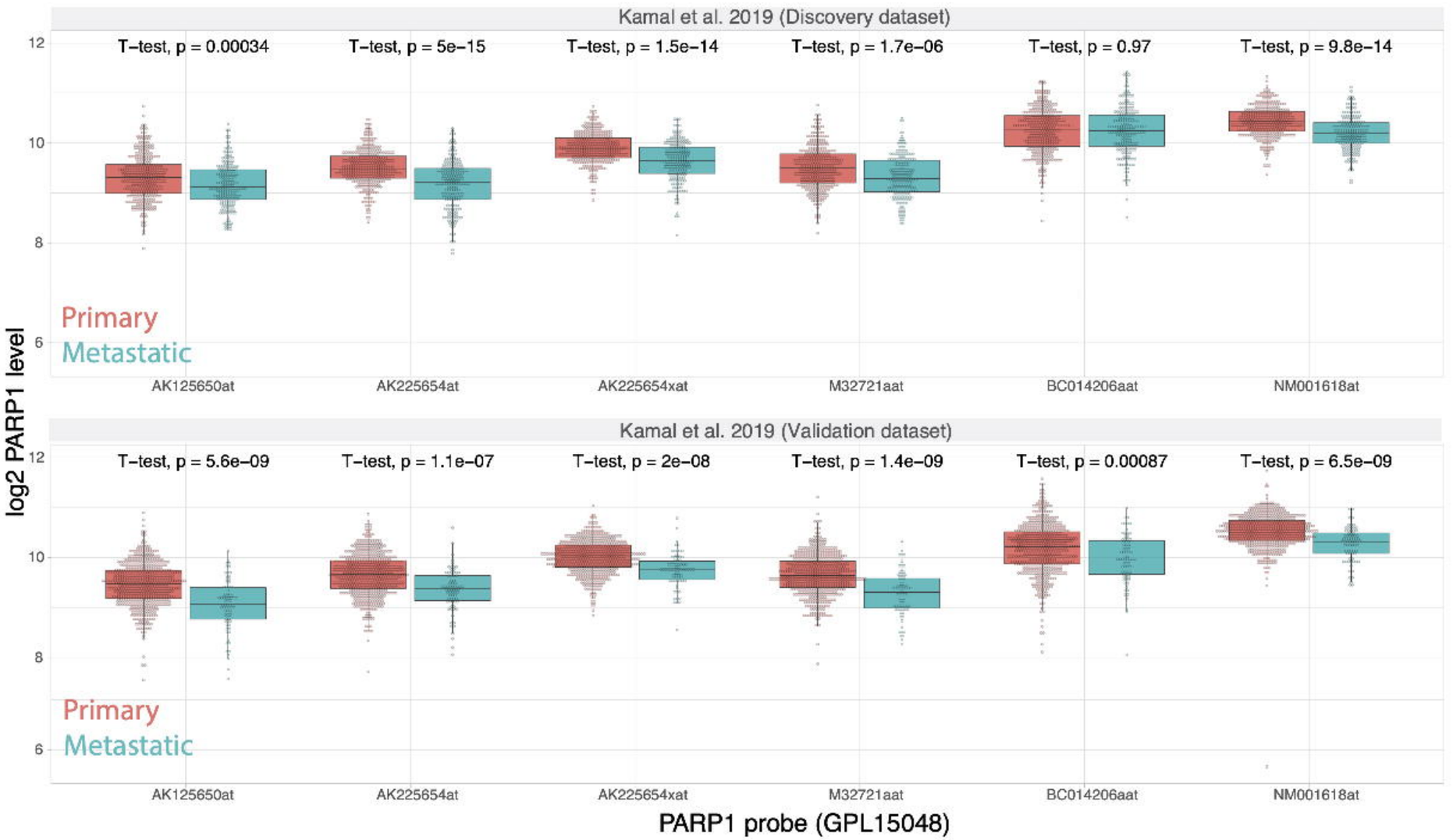

Figure S5

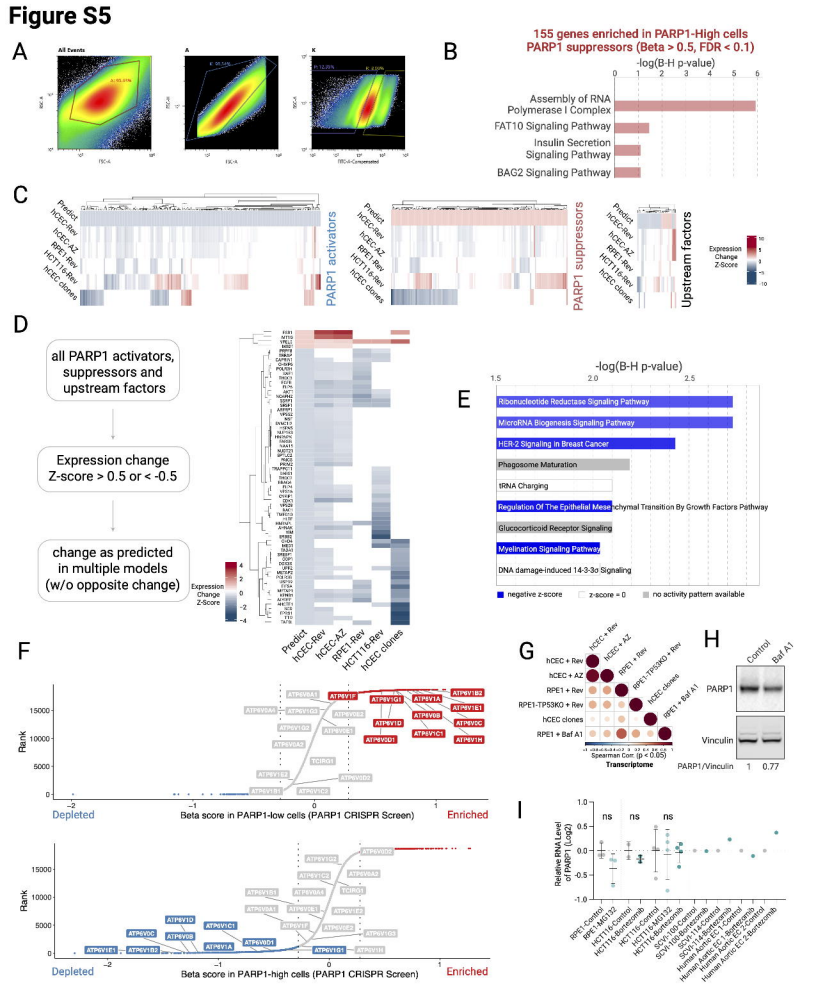
A
All Events
A
K
FSC-A
SSC-A
FSC-A-Compensated
B
155 genes enriched in PARP1-High cells
PARP1 suppressors (Beta > 0.5, FDR < 0.1)
-log(B-H p-value)
Assembly of RNA Polymerase I Complex
FAT10 Signaling Pathway
Insulin Secretion Signaling Pathway
BAG2 Signaling Pathway
C
Predict
hCEC-Rev
hCEC-AZ
RPE1-Rev
HCT116-Rev
hCEC clones
PARP1 activators
PARP1 suppressors
Upstream factors
Expression Change Z-Score
D
all PARP1 activators, suppressors and upstream factors
Expression Change Z-Score > 0.5 or < -0.5
change as predicted in multiple models (w/o opposite change)
Expression Change Z-Score
E
-log(B-H p-value)
Ribonucleotide Reductase Signaling Pathway
MicroRNA Biogenesis Signaling Pathway
HER-2 Signaling in Breast Cancer
Phagosome Maturation
tRNA Charging
Regulation Of The Epithelial Mesenchymal Transition By Growth Factors Pathway
Glucocorticoid Receptor Signaling
Myelination Signaling Pathway
DNA damage-induced 14-3-3σ Signaling
negative z-score
z-score = 0
no activity pattern available
F
Rank
Depleted
Beta score in PARP1-low cells (PARP1 CRISPR Screen)
Enriched
Beta score in PARP1-high cells (PARP1 CRISPR Screen)
G
Spearman Corr. (p < 0.05)
Transcriptome
H
Control
Baf A1
PARP1
Vinculin
PARP1/Vinculin
1
0.77
I
Relative RNA Level of PARP1 (Log2)
ns

Figure S6

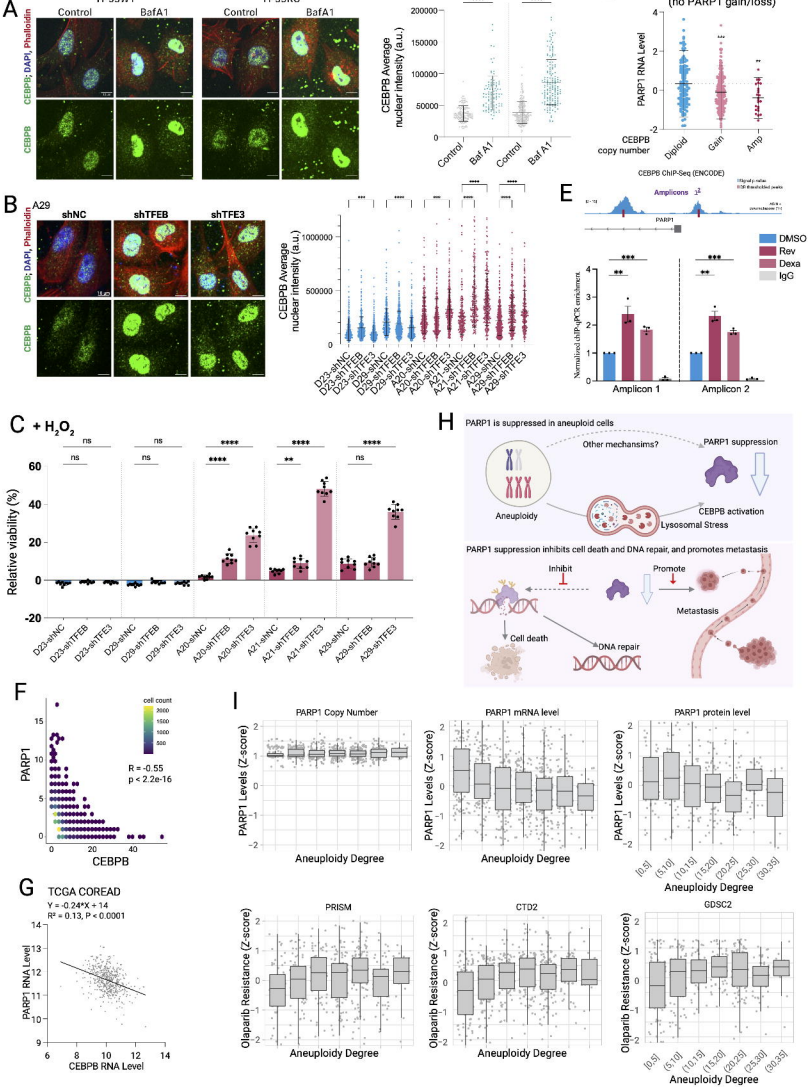

A
TP53WT
TP53KO
Control
BafA1
CEBPB; DAPI, Phalloidin
CEBPB
CEBPB Average nuclear intensity (a.u.)
Control
Baf A1
D
TCGA COREAD (no PARP1 gain/loss)
PARP1 RNA Level
CEBPB copy number
Diploid
Gain
Amp
B
A29
shNC
shTFEB
shTFE3
CEBPB Average nuclear intensity (a.u.)
D23-shNC
D23-shTFEB
D23-shTFE3
D29-shNC
D29-shTFEB
D29-shTFE3
A20-shNC
A20-shTFEB
A20-shTFE3
A21-shNC
A21-shTFEB
A21-shTFE3
A29-shNC
A29-shTFEB
A29-shTFE3
E
CEBPB ChIP-Seq (ENCODE)
Amplicons
PARP1
DMSO
Rev
Dexa
IgG
Normalized chIP-qPCR enrichment
Amplicon 1
Amplicon 2
C + H_2O_2
Relative viability (%)
H
PARP1 is suppressed in aneuploid cells
Other mechansims?
PARP1 suppression
Aneuploidy
CEBPB activation
Lysosomal Stress
PARP1 suppression inhibits cell death and DNA repair, and promotes metastasis
Inhibit
Promote
Metastasis
Cell death
DNA repair
F
cell count
R = -0.55
p < 2.2e-16
PARP1
CEBPB
I
PARP1 Copy Number
PARP1 mRNA level
PARP1 protein level
PARP1 Levels (Z-score)
Aneuploidy Degree
G
TCGA COREAD
Y = -0.24*X + 14
R² = 0.13, P < 0.0001
PARP1 RNA Level
CEBPB RNA Level
PRISM
CTD2
GDSC2
Olaparib Resistance (Z-score)